SYNTHESIS, CHARACTERIZATION AND TOXICITY OF BIOCONJUGATED CdS QUANTUM DOTS

A DISSERTATION

Submitted in partial fulfillment of the

requirements for the award of the degree

of

MASTER OF TECHNOLOGY

in

NANOTECHNOLOGY

By

ANKUR ANAND

CENTRE OF NANOTECHNOLOGY
INDIAN INSTITUTE OF TECHNOLOGY ROORKEE
ROORKEE – 247 667 (INDIA)

JUNE, 2010

CANDIDATE'S DECLARATION

I hereby declare that the work, which is presented in this dissertation titled, " **Synthesis, Characterization and Toxicity of Bioconjugated CdS quantum dots** " in the partial fulfillment of the requirements for the award of degree of **Master of Technology** in **Nanotechnology** submitted in the Centre of Nanotechnology, Indian Institute of Technology Roorkee, Roorkee, is an authentic record of my own work carried out from July 2009 to June 2010, under the supervision and guidance of **Dr. Raj Kumar Dutta**, Assistant Professor, Department of Chemistry, Indian Institute of Technology Roorkee, Roorkee.

I have not submitted the matter embodied in this dissertation for the award of any other degree.

Date: 30-06-10

Place: Roorkee **(ANKUR ANAND)**

CERTIFICATE

This is to certify that the above statement made by the candidate is correct to the best of my knowledge and belief.

Date: 30/6/10

Place: Roorkee **(Dr.R.K. Dutta)**

Assistant Professor,
Department of Chemistry,
Indian Institute of Technology Roorkee,
Roorkee – 247 667

Acknowledgement

I would like to take this opportunity to extend my heartfelt gratitude to my guide and mentor **Dr. R.K. Dutta**, Associate Professor, Department of Chemistry, Indian Institute of Technology Roorkee, for his trust in my work, his able guidance, and regular source of encouragement and assistance throughout this dissertation work. I would state that the dissertation work would not have been in the present shape without his inspirational support and I consider myself fortunate to have done my dissertation under him.

I also extend my sincere thanks to **Dr. Anil Kumar**, Professor and Head of the Department of Centre of Nanotechnology, for providing facilities for the work. I would like to thank all my friends who supported and encouraged me to finish this work.

Ankur Anand

Abstract

Thiol stabilised CdS quantum dots were prepared by arrested precipitation method. The method is simple, reproducible and developed at room temperature. The quantum dots thus produced were stable for months. The resultant CdS quantum dots were functionalised with lactoferrin by means of coupling chemistry. These quantum dots were characterized by UV–VIS, fluorescence spectroscopy; Fourier transformed infrared spectroscopy, X-ray diffraction (XRD), Scanning electron microscopy (SEM) and atomic force microscopy (AFM).

The effect of toxicity of quantum dots on *E. coli* was done and both CdS quantum dots and lactoferrin functionalised quantum dots resulted in inhibition of growth of *E.coli.*

TABLE OF CONTENTS

LIST OF FIGURES

Chapter 1

Introduction

1.1 General Introduction

Quantum dots are inorganic semiconductor nanocrystals whose sizes are smaller than the Bohr exciton radius. Their excitons (electron-hole pair) are spatially confined in all three dimensions. As a result, they have properties that are between those of bulk semiconductors and those of discrete molecules. These are nanocrystals composed of elements from groups of II-VI, III-V, or IV-VI of periodic table. The termed quantum dot is coined by the Mark reed in a paper published in 1988 (1). What makes quantum dots (QDs) such unusual objects is, first of all the possibility of controlling their shape, their dimensions, the structure of energy levels and number of confined electrons. It is possible for instance, to create and investigate such school models as a rectangular or parabolic potential well, the radiative recombination from a few-particle system, and so on. The small number of electrons in typical quantum dot, which facilitates carrying out the ab-initio calculations, makes these systems, mini-laboratories of many body physics, particularly attractive for theoretical physicists. Some intriguing effect characteristics of two-dimensional electronic systems such as formation of the composite fermions, which led to the fractional quantum Hall effect seems also to occur in quantum dots, where the possibility of numerically solving Schrödinger equation held a great promise.

Current experiments concerned with quantum dots focus mainly on studying their optical properties (absorption and emission of light in a visible or far infrared range, and Raman

scattering of light) and electric properties (capacitance and Transport studies). Since quantum dots absorb and emit light in a very narrow spectral width, it seems that they might very soon find application in the construction of more efficient and more precisely controllable semiconductor lasers. The first experimental results and (2, 3) and theoretical expectations are very promising.

A fascinating idea of great promise is that of observing the formation of the band structure in a crystal lattice consisting of a great number (10^8) of uniformly separated, identical size and shape quantum dots (4). What is also promising is the possibility of an application of quantum dots in a so called quantum computers.

1.2 History

In 1932 H.P. Roksby (5) discovered that the red and yellow colour of some silicate glasses could be linked to the microscopic inclusions of CdSe and CdS. It was not until 1985 when these changes in colour were linked to the energy states determined by the quantum confinement in these CdSe or CdS quantum dots (6). By the end of 1980s the main properties of quantum wells and super lattices were well understood and the interests of the researchers were shifted towards structures with further reduced dimensionality to quantum wires (Kapon 1989) and then further to quantum dots. Complete quantization of the electron's free motion was implemented by trapping it in a quasi-zero dimensional quantum dot. This was first achieved by scientist from Texas Instruments Incorporated. Reed et al (7) reported the creation of a square quantum dot with a side length of 250 nm, etched by means of lithography. Subsequent publications reporting the creation of quantum dots in others research centers soon appeared. The first among those are AT &T Bell Laboratories (8,9) and Bell Communication Research Incorporated (10). The diameters of these dots were already

much smaller: 30-45 nm. Complete reduction of quantum wells to quantum dots leads to the carrier localization in all three dimensions and breakdown of classical band structure model of a continuous dispersion of energy as a function of momentum. The resultant energy levels of the quantum dots is discrete, like in atoms in many respects if not all and therefore quantum dots are frequently referred to as the artificial atoms, superatoms, or quantum dots atoms. The typical size of such a dot is 10 nm and it still contains 10^4 or more atoms. A profound size-dependent change of all macroscopic properties as compared to the bulk occurs. Figure1 .1 illustrates the evolution of quantum dots and its property from that of bulk and earlier nanostructures.

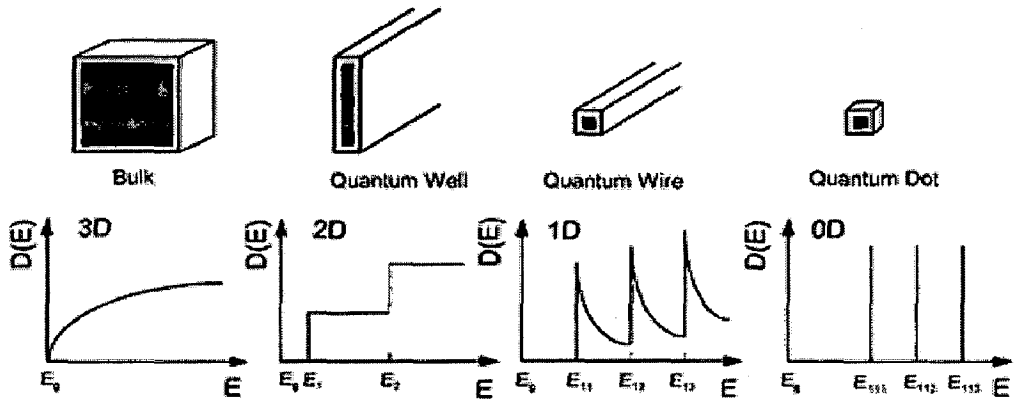

Figure 1.1 Evolution of electronic properties of semiconductor nanostructures as compared to bulk semiconductor

Not surprisingly, nature had provided us with quantum dots even before we knew what to call them. The uses of Gold (Au), Silver (Ag), Cadmium (Cd), and Sulphur (S), Selenium (Se), among others were well known among the glassmakers of the antiquity as additives to produce the colour. These have been commercially available as colour filters for the decades. Quantum confinement's effects in such a system were confirmed experimentally by Ekimov and Onushenko (1984). The early pioneering work with respect to fabrications and properties

of quantum dots was attributed to Efros (11), Brus (12), Reed (13) and Weller et al (14). What has peaked and sustained the scientific interest are the many new methods that have been brought to bear to produce such structures.

Clearly in earlier years, the combination of high resolution electron lithography and Molecular Beam Epitaxy (MBE) has played a major role. Later on, with the advent of synthesis of colloidal quantum dots, the door becomes open to the role of quantum dots as an imaging agent in the biology. Since then quantum dots have found many applications in the fields as diverse as solar cells, quantum dot lasers, single electron devices, light emitting diodes (LEDs), quantum computing, imaging agents and diagnostics. Figure 1.2 illustrates the growing popularity of quantum dots.

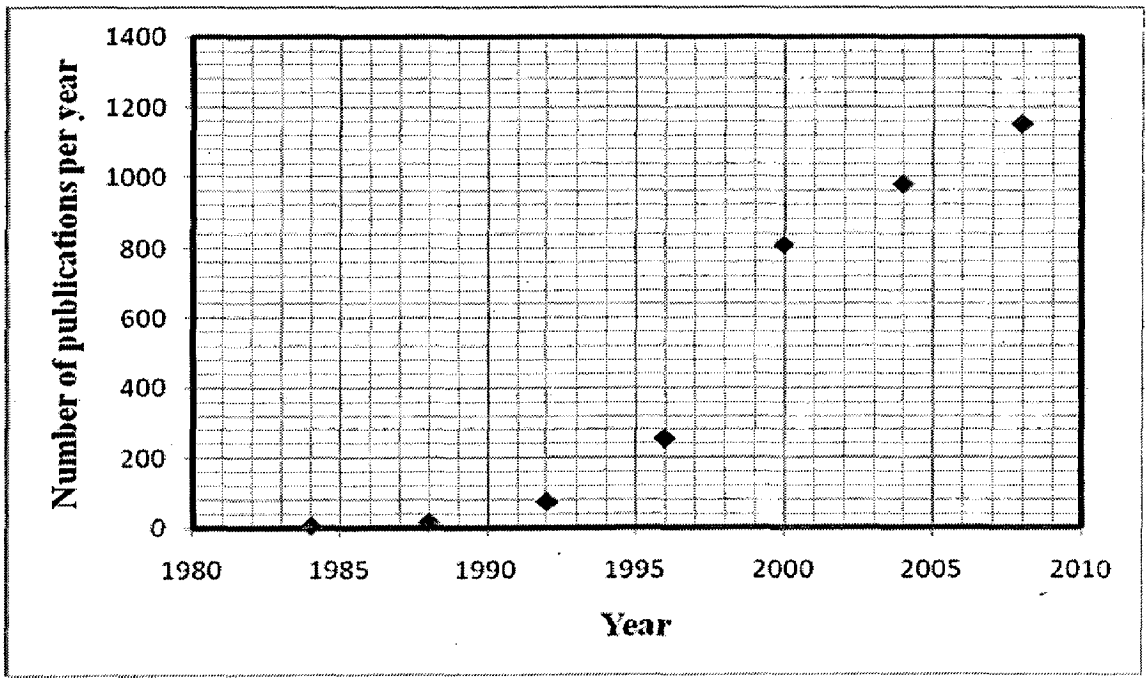

Figure 1.2 Number of publications containing the term "quantum dots" yearwise.

Figure 2 shows the predicted evolution of the minimum semiconductor device feature according international Technology roadmap for the semiconductor heterostructures (15).

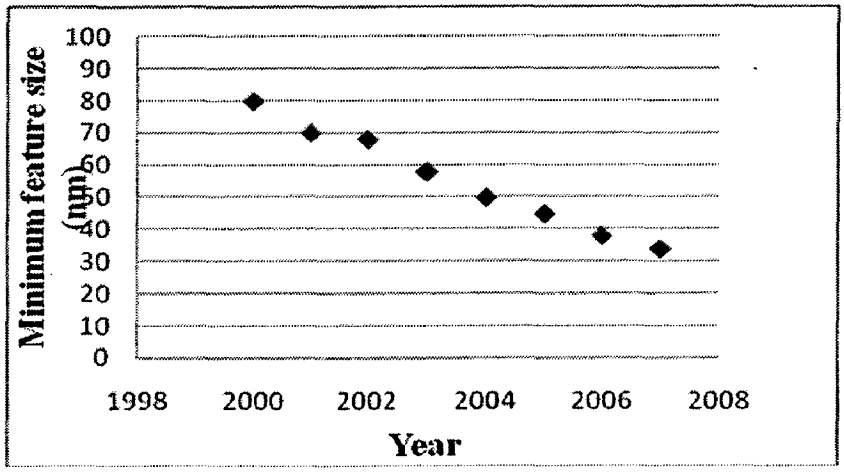

Figure 1.3 Minimum feature sizes

Colloidal quantum dots emerged from a number of research labs in the early 1980s, with Louis Brus being singled out to receive the first Kavli Prize in Nanoscience in 2008 for his pioneering efforts in this field (16, 17). The preparation of II–VI semiconductor nanoparticles started with the work published by A. Henglein in 1982 (18) Like others (19,20), this paper deals with surface chemistry, photodegradation, and catalytic processes in colloidal semiconductor particles. But it is this very work which reveals the first absorption spectrum of a colloidal solution of size-quantized CdS nanocrystals.

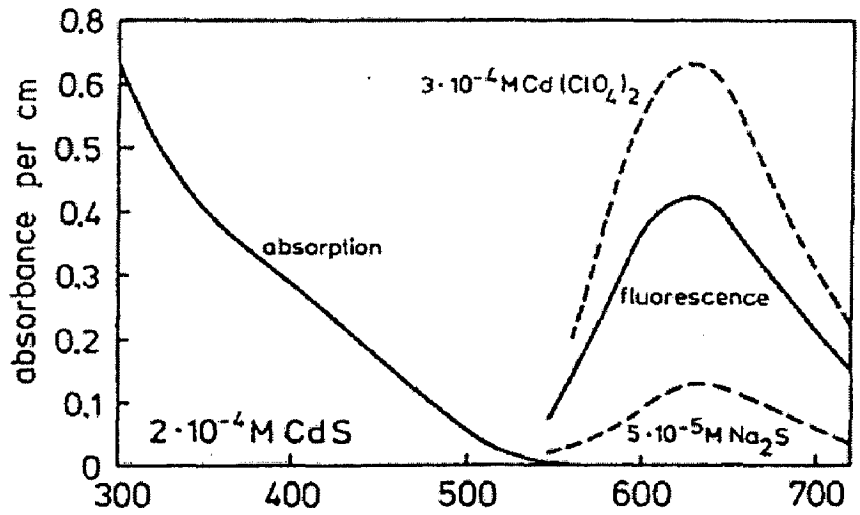

Figure 1.4 Absorption and emission spectrum of colloidal CdS Solution. (1)

These were prepared from Cd $(ClO_4)_2$ and Na_2S on the surface of commercial silica particles. As seen from Figure 1.4, the absorption onset is shifted considerably to higher energies with respect to the bulk band gap of CdS (515 nm). In addition, the sol emits light upon excitation at 390 nm, which is also a matter of investigation in this paper.

The first correct interpretation of the observed blue shift of the absorption as a quantum mechanical effect was due to L. Brus (21). In the framework of the effective mass approximation, the shift in the kinetic energy of the charge carriers due to their spatial restriction to the volume of the nanometre-sized semiconductors was calculated. The comparable experimental (22) and theoretical work (23) was carried out at almost the same time on the I–VII compound CuCl in the Soviet Union.

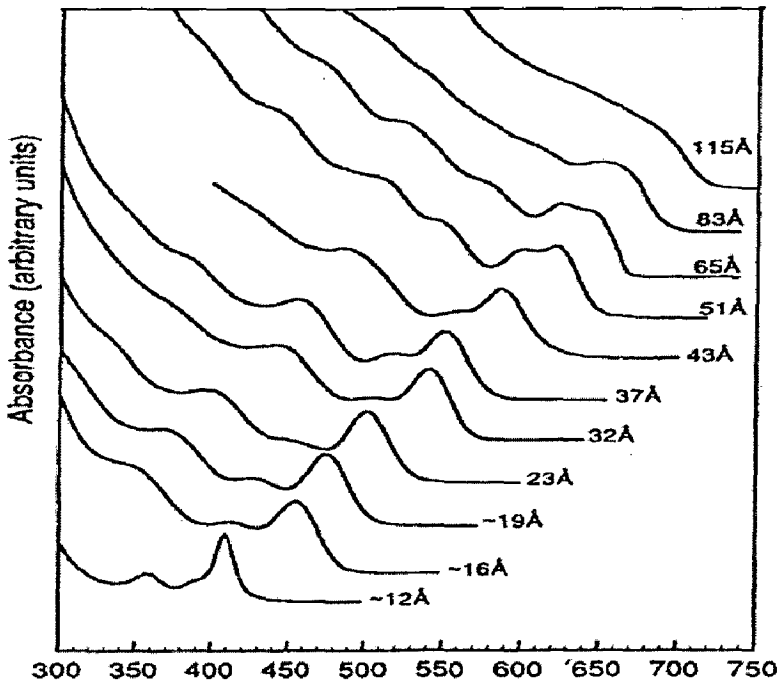

Figure 1.5 Absorption spectra of CdSe colloidal solutions (TOP-TOPO synthesis) (11).

From then on there is increasingly attention on the colloidal synthesis of quantum dots, with different kinds of capping agents because of reasons mentioned below:

1. Quantity of quantum dots can be obtained from colloidal synthesis methods as compared to lithographic techniques.
2. Better control of size and shape and hence optical and electronic properties.
3. Water-soluble quantum dots can only synthesized in colloidal solutions for biological applications.
4. Quantum dots synthesize from colloidal means gave advantages to be amenable for tinkering with various coatings which cannot seem possible by means of physical techniques of fabricating them.
5. The possibility of formation of superstructures, for example, core-shell quantum dots, quantum dot-quantum well heterostructure etc.

Physicists on other hand concentrate on the synthesis of quantum dots with lithographic techniques since that would allow them to investigate the properties of quantum dots on single dot level. Besides this, quantum dots synthesized by physical means shows less or no edge defects and hence becomes ideal candidates for understanding quantum mechanical phenomena in which physical solving Schrodinger equation for such system hold great promise.

The First biological applications of quantum dots were reported in 1998 (24,25) Bruchez et al. (24) and Chan and Nie (25) used CdSe QDs coated with silica and mercaptoacetic acid layers respectively, in order to rendered QDs water soluble, and both groups showed specific labeling by covalent coupling of ligands to these surfaces. Subsequently, several authors have reported labeling of whole cells and tissue sections using several different surface modifications of QDs (26-29). By attaching biomolecules to nanometer-sized bits of semiconductors, a sensitive and potentially widely applicable method for detecting biomolecules and for scrutinizing bimolecular interactions inside the cell can be relised.

1.3 Fabrication or synthesis of quantum dot.

Broadly speaking, there are two ways of synthesizing quantum dots. While chemists prefer to use 'wet' methods to produce relatively large volumes of colloidal quantum dots, which are usually passivated by organic molecules on their surface, physicists, on the other hand, tend to work with epitaxial quantum dots that are painstakingly defined by electrostatic gates on substrates, or that self-assemble on surfaces.

Based on above argument there are broadly two approaches for fabrication or synthesis of quantum dots.

1. Top-Down Approach
2. Bottom-up Approach

The methods comprising the former class are physical methods for fabricating quantum dots but strictly speaking not all physical methods are top-down method while later class of methods is essentially comprises of synthesis by means of chemical agents.

1.3.1 Top- Down approach

In Top-down approach, there are several methods for fabricating quantum dots namely etching, modulation of electric field, interdiffusion between barrier and quantum well, self-organized growth and selective growth. These methods are briefly explained below.

1.3.1.1 Etching

The earliest method of obtaining quantum dots was implemented by Reed et al. (30), who etched them in a structure containing two-dimensional electron gas or quantum well, The steps in this process is shown in Figure 1.6 The surface of sample containing one or more quantum wells is covered by the polymer mask, and then partly exposed (Figure. 1.6a). The

exposed pattern corresponds to the shape of the created nanostructure. Because of the required high resolution, the mask is not exposed to the visible light, but to the electron or ion beam (electron/ion beam lithography). At the exposed areas the mask is removed (Figure 1.6b). Later, the entire surface is covered with a thin metal layer (Figure 1.6c). Using special solution, the polymer film and the protective metal layer are removed, and a clean surface of the sample is obtained, except for the previously exposed areas, where the metal layer remains (Figure 1.6d). Next by chemically etching the areas not protected by the metal mask (Figure 1.6e), the slim pillars are created, containing the cut-out fragments of quantum wells (Figure 1.6f).

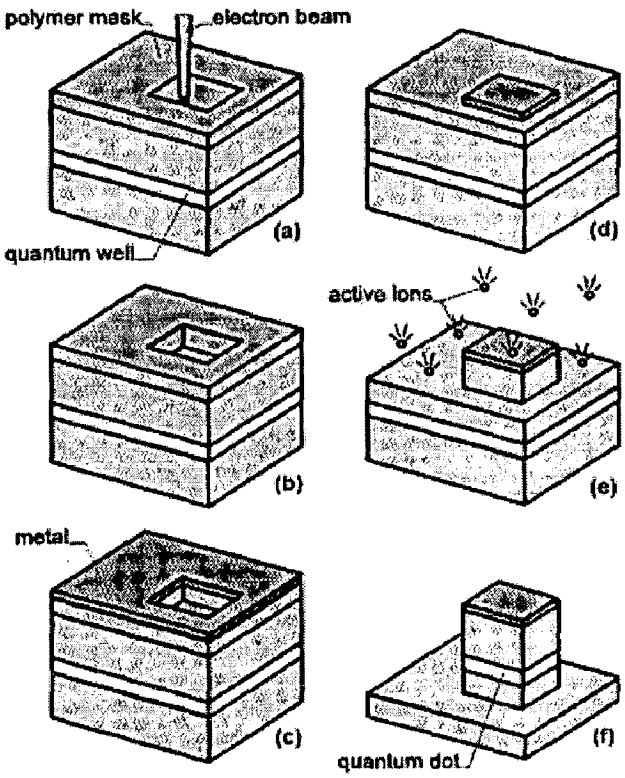

Figure 1.6 (a-f) Process of quantum dot etching (31)

In this way the motion of the electrons, which is initially confined in the plane of the quantum well, is further restricted to a small pillar with a diameter on the order of 10-100 nm.

The chromium doped gallium arsenide (GaAs) base serves as a source of free carriers, 333which flow into multiple GaAs quantum wells, created above the buffers layers and separated by the aluminum-gallium arsenide (AlGaAs) barriers. The etching depth drops beneath the interface between the last quantum well and the buffer layer. The gold mask that remains after the etching process may serve as the electrode. The voltage applied to the electrode controls the number of carriers confined in the dots.

1.3.1.2 Modulated electric field

Another method consists in the creation of miniature electrodes over the surface of quantum wells by means of lithographic techniques, as shown in Figure. 1.7. The application of an appropriate voltage to the electrodes produces a spatially modulated electric field, which localizes the electron within a small area. The lateral confinement created in this way shows no edge defects, which are characteristics of such edge structures.

The process of spreading thin electrodes over the surface of a quantum well may produce both single quantum dots (32) and large arrays (matrixes) of dots (33, 34). When a voltage is applied to the electrodes, the result is a change in the both dot size and the depth of the confining potential. The potential depth influences the number of confined electrons.

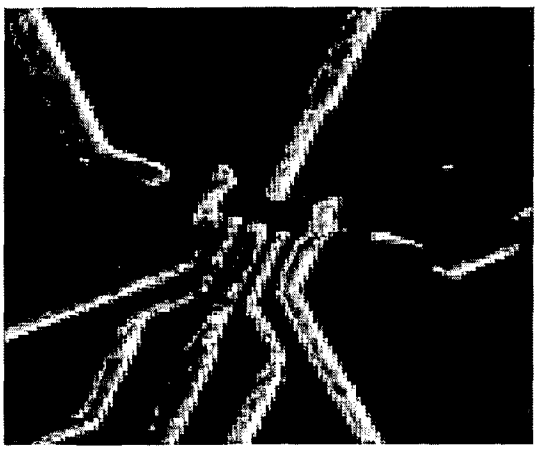

Figure 1.7 Quantum dot on the intersection of electrodes

1.3.1.3 Interdiffusion between the barrier and the quantum well

Brunner et al. (35) describe a method for obtaining quantum dots based on quantum-well material by local heating of sample with a laser beam. A parent material of a single, 3 nm thick GaAs quantum well was used, and this was prepared using the molecular beam epitaxy method (MBE). It was then placed between the pair of 20 nm thick $Al_{0.35}Ga_{0.65}As$ barriers. The topmost 10 nm thick GaAs cap layer was covered with a 100 nm coating of Si_3N_4, protecting the surface against the oxidation and melting by the laser beam. At a temperature of about 1000 °C a rapid interdiffusion of Al and Ga atoms occurred between the well and the barriers, which led to the creation of a local modulation of the material band structure with the creation of the potential barrier. It has been observed that for the dimensions near 450 nm the effective potential confining electrons is closed to an isotropic parabola.

1.3.1.4 Self-organized growth

Petroff and Denbaars (36) describe another method for creation of quantum dots that does not require the creation of mask. When the lattice constants of the substrate and the crystallized material differ considerably (7% in the case of GaAs and InAs, the most commonly used pair of compounds), only the first deposited monolayers crystallized in the form of epitaxial, strained layers with the lattice constant equal to that of the substrate. When the critical thickness is exceeded, a significant strain occurring in the layers lead to the break-down of such an ordered structure and to the spontaneous creation of randomly distributed islets of regular shape and similar sizes. The shape and average size of islets depends mainly on the factors such as the strain intensity in the layer as related to the misfit of lattice constants, the temperature at which the growth occurs, and the growth rate. The phase transition from the epitaxial structure to the random arrangement of islets is called the

Stransky-Krastanov transition (37). The quantum dots formed in the Stransky-Krastanov phase transition are called self-organized or self-assembled quantum dots (SAD). Figure 1.8 presents the dependence of the critical number of InGaAs monolayer's deposited on GaAs substrate, at which the phase transition occurs, on the indium concentration in the solution (Lower axis), or alternatively the misfit of lattice constant (upper axis) that is strain.

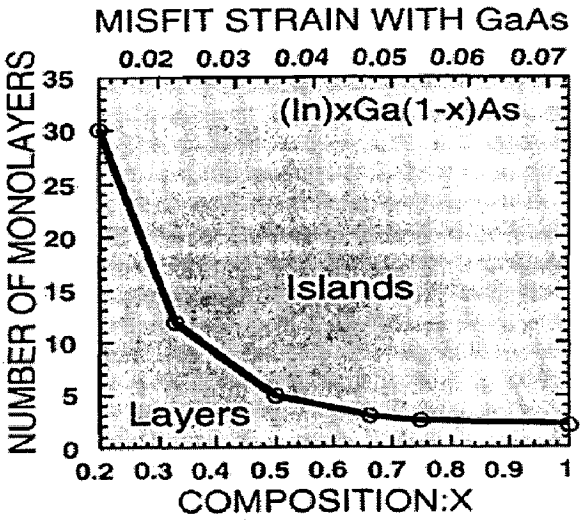

Figure 1.8 Dependence of the critical thickness of the InGaAS layer, at which the Stransky-Krastanov phase transition takes place, on the Indium concentration (i.e., the strain) (37).

According to the Figure 1.8 the transition occurs at the 1.8 monolayer deposition. When the process of crystallization is terminated shortly after reaching the phase transition, the islets evolve to the state of quasi-equilibrium, in which they assume the shapes of pyramids (38,39) or flat, circular lenses (40, 41) formed on a thin layer of InGaAs (the wetting layer).

The small sizes of the self-assembled quantum dots, homogeneity of their shapes and sizes in a macroscopic sample, perfect crystal structure (without edge defects), and the fairly convenient growth process, without the necessity of the precise deposition of electrodes or etching are among the greatest advantages.

1.3.1.5 Selective growth

Quantum dots can also be created through the selective growth of a semiconducting compound with narrower band gap (e.g., GaAs) on the surface of another compound with wider band gap (e.g., AlGaAs) (42). The restriction of the growth areas is obtained by covering the surface of the sample with a mask (SiO_2) and etching on it miniatures triangles. On the surface that is not covered with the mask the growth is then carried out with the metal-organic chemical vapour deposition method (MOCVD), at a temperature of 700-800 °C. The crystals that are created have the shape of tetrahedral pyramids, and only the top of the pyramid is created of GaAs layer with bottom most layers is of substrate (AlGaAs). It is possible to obtain a dot of effective size below 100 nm. The pictures of such dots are shown in Figure 1.9

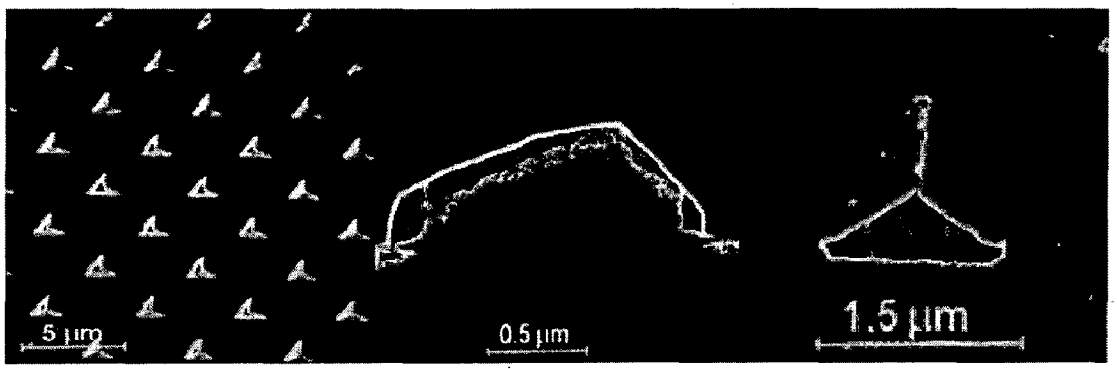

Figure 1.9 Quantum dots created on the surface of GaAs in selective MOCVD growth.

1.3.2 Bottom-up Approach.

Bottom-up approach for synthesizing quantum dots or semiconductor nanocrystals essential comprises of chemical colloidal synthesis.

1.3.2.1 Chemical synthesis

The synthesis of quantum dots by chemical routes can be done by different methods namely sol-gel synthesis, arrested precipitation method, sonochemical method, hydrothermal method and microwave-assisted method. The following account gives brief introduction to the synthesis of quantum dots from above mentioned chemical methods.

1.3.2. 1a. Sol-Gel method

The sol-gel process, also known as chemical solution deposition, is a wet-chemical technique widely used in the fields of materials science and ceramic engineering. Such methods are used primarily for the synthesis of materials from a chemical solution which acts as the precursor for a gel of discrete particles. Typical precursors are metal alkoxides and metal chlorides, which undergo various forms of hydrolysis and polycondensation reactions. Thus, the sol evolves towards the formation of a gel-like diphasic system containing both a liquid phase and solid phase. Removal of the remaining liquid (solvent) phase requires a drying process, which is typically accompanied by a significant amount of shrinkage and densification. The rate at which the solvent can be removed is ultimately determined by the distribution of porosity in the gel. Afterwards, a thermal treatment, or firing process, is often necessary in order to favour further polycondensation and enhance mechanical properties and structural stability via final sintering, densification and grain growth. Mackenzie et al (43) reported the synthesis of CdS quantum dots via sol-gel process in glass. In that paper they

reported optical gain of synthesized quantum dot and attributed it to the recombination of several excited levels between two and one electron-hole pairs states (i.e., biexciton to exciton). A sol-gel method for synthesis of InP nanocrystals embedded in silica glasses was described by Yao et al. Gels were synthesized by hydrolysis of a complex solution of $Si(OC_2H5)_4$, $InCl_3.4H_2O$, and $PO(OC_2H_5)_3$. The size of InP nanocrystals was found to be from 2 to 8 nm in diameter with strong photoluminescence peak at 856 nm (44).

1.3.2.2 Sonochemical method

In sonochemical method, ultrasound waves of around 20 Kilohertz (KHz) radiation breaks the chemical bonds from the temperature that created due to implosive collapse of bubbles in the solution. The main event in the sonochemistry is creation, growth and collapse of the bubble that is formed inside the liquid. The temperature of about 5000 °C formed inside the cavitation bubble and of 1900 °C at the interface of cavitation bubble. The heating and cooling rates around bubbles are over 10^{10} Kelvin/second. These extreme conditions caused the rupture of the chemical bonds. The width of interfacial region which surrounds the collapsing bubble was calculated to around 200 nm. Sonochemical synthesis of nanoparticles are based on the decomposition of metal precursor (usually a metal carbonyl complexes) dissolved in a high-boiling solvent under irradiation with high intensity ultrasound. In the presence of stabilizing agents these atoms agglomerate to nanosized particles (45). The products are either amorphous or crystalline nanoparticles depending on the temperature in the ring region where the reaction takes place (46). The sonochemical driven synthesis of CdSe quantum dots (QDs) and their subsequent sonochemical ZnS shelling was done by Long et al. (47). They used $Cd(OAc)_2$, TOPO, and hexadecylamine in ultrasound bath and subsequent sonochemical ZnS shelling procedure to CdSe QD cores using Zn-ethylxanthate to produce highly luminescent QDs with quantum yields of 50% to 60%, narrow emission

spectra (48). Hexagonal CdSe and CdS nanoparticles was prepared using $Cd(Ac)_2$ and less hazardous elemental Se or S as precursors, respectively, with the aid of ultrasound irradiation under an atmosphere of H_2/Ar (5/95, V/V%). The products of reaction consist of 7–10 nm nanocrystallites which aggregated in the form of polydispersive nanoclusters with sizes in the range 30–40 nm in the case of CdSe, and near monodispersive nanoclusters with a mean size of about 40 nm in the case of CdS (49)

1.3.2.3 Hydrothermal method

Hydrothermal synthesis includes the various techniques of crystallizing substances from high-temperature aqueous solutions at high vapor pressures; also termed "hydrothermal method". It can be defined as a method of synthesis of single crystals which depends on the solubility of chemicals in hot water under high pressure. The crystal growth is performed in an apparatus called autoclave, in which precursors are supplied along with water. A gradient of temperature is maintained at the opposite ends of the growth chamber so that the hotter end dissolves the nutrient and the cooler end causes seeds to take additional growth [wikipedia].

Possible advantages of the hydrothermal method over other types of crystal growth include the ability to create crystalline phases which are not stable at the melting point. Also, materials which have a high vapor pressure near their melting points can also be grown by the hydrothermal method. The method is also particularly suitable for the growth of large good-quality crystals while maintaining good control over their composition. For hydrothermal experiments the requirements for starting materials are

(i) Accurately known composition,

(ii) As homogeneous as possible,

(iii) As pure as possible and

(iv) As fine as possible (50).

A simple hydrothermal method for the synthesis of CdTe quantum dots was done by mixing aqueous solution of NaHTe, thioglycollic acid and $CdCl_2$ into the polytetrafluoroethylene pot and subsequently heating them at temperatures ranges from 100 °C to 200 °C with difference of 20 °C. The synthesized nanoparticles were reported to have size range of 2-6 nm depend upon concentration of precursors and temperature and with high photoluminescence efficiency of 27.4% at room temperature (51) Yitai quin et al reported the synthesis of Indium phosphide (InP) nanocrytals by hydrothermal method. In this procedure they mixed $InCl_3.4H_2O$, excess yellow phosphorus, $NaBH_4$ and potassium stearate ($C_{17}H_{35}CO_2K$) into 50 mL of aqueous ammonia and after stirring the solution was transferred into a stainless steel Teflon-lined autoclave which was sealed and maintained at 140 °C for 8–12 h with subsequent cooling to the room temperature. The quantum dots so synthesized were spherical in shape and emission maxima at 685 nm at room temperature (52).

1.3.2.4 Microwave-assisted method

Microwaves act as high frequency electric fields and will generally heat any material containing mobile electric charges, such as polar molecules in a solvent or conducting ions in a solid. Polar solvents are heated as their component molecules are forced to rotate with the field and lose energy in collisions. Semiconducting and conducting samples heat when ions or electrons within them form an electric current and energy is lost due to the electrical resistance of the material.

1.4 Physics of quantum dots

1.4.1 Electronic property of quantum dots

Semiconductor nanocrystals are novel materials with properties lying between the molecular and solid-state regimes, these properties, uniquely, being controlled by size and shape. Containing hundreds to thousands of atoms, 2–20 nm in diameter, nanocrystals maintain a crystalline core with the periodicity of the bulk semiconductor. However, as the wave functions of electrons and holes are confined by the physical nanometric dimensions of the nanocrystals, the structure of the electronic levels and the resultant optical and electrical properties are greatly modified. Upon reducing the semiconductor size to the nanocrystal regime, a characteristic blue shift of the band gap appears, and a discrete level structure develops as a result of the ''quantum size effect'' in these quantum structures (53). In case of semiconductor nanocrystals this happens when there dimension is comparable to "Bohr exciton radius". An exciton is quasiparticle consisting of a bound state of an electron and imaginary particle called hole in semiconductor. Exciton formation may occur when a photon enter a semiconductor, excites the electron from valence band to conduction band leaving a hole behind previously occupied site of electron in valence band. As such, it is coulomb correlated electron-hole pair with no net charge. The distance between electron and hole within an exciton is known as "Bohr exciton radius". The Bohr exciton radius is given by the expression,

$$a_{e,h} = \frac{\hbar^2 \kappa}{\mu e^2}$$

here, $\hbar$ is reduced Plank constant, κ is wave number (vector), μ is reduced mass of electron-hole system and is given by,

$$\mu = \frac{m_e^* m_h^*}{m_e^* + m_h^*}$$

where, m_e^* and m_h^* are the effective mass of the electron and hole respectively.

Table 1.1 gives calculated results of Bohr exciton radius of various semiconductor quantum dots based on above equation.

Quantum dot	Electron effective mass (m^*_e)	Hole effective mass (m^*_h)	Reduced mass (μ)	Exciton radius (nm)
CdSe	0.13	0.45	0.108	6.1
CdS	0.21	0.68	0.16	3.4
ZnS	0.34	1.76	0.29	1.8
GaAs	0.067	0.082	0.036	21.6
InSb	0.014	0.42	0.013	78.5

Table 1.1 Bohr exciton radius of various semiconductor quantum dots.

The size of the quantum dot with respect to its Bohr exciton radius allow us to classify them into region of different confinements as shown in Table 1.2

CONFINEMENT	SIZE	EFFECT
Weak	$a > a_e, a_h$	$E_{conf} < E_{coul}$, Exciton confined with $m^* = m_e + m_h$
Intermediate	$a_{e,(h)} > a > a_{h,(e)}$	$E_{conf\,e,(h)} > E_{coul}$, Electron (hole) confines with $m^* = m_{e,(h)}$ Only conduction (valence) states are discrete
Strong	$a_{e,h} > a$	$E_{conf\,e,h} > E_{coul}$, Both electron and hole are confined, Both valence and conduction levels are discrete

Table 1.2 Different regimes of confinement

In table 'a' is size of semiconductor nanocrystal, '$a_{e,(h)}$' is Bohr radius of electron or hole, 'E_{conf}' stands for confinement energy and 'E_{coul}'stands for columbic energy between electron and hole.

There are several models such as effective mass approximation, tight binding approach, empirical pseudo-potential method and ab-initio methods which describes the energy states of electron and holes in semiconductor nanocrystal. Each has its own advantages and disadvantages. However for the sake of simplicity, effective mass approximation method is briefly described here.

The interaction between electrons and holes in a quantum dot can be described by solving Hamiltonian for this system. However the formulation of actual physical situation is more complicated than the electron in 3-D box because here we must consider the electron and the hole separately, as well as their interaction besides influence of periodic potential of crystal lattice. As a consequence, the Hamiltonian must also include separate energy terms for the electron and the hole, as well as a columbic term to account for their mutual interaction and hence the Hamiltonian for the system can be written as (56)

$$H = -\frac{\hbar^2}{2m_e^*}\nabla_e^2 - \frac{\hbar^2}{2m_h^*}\nabla_h^2 - \frac{e^2}{\varepsilon_r |r_e - r_h|} + U(r)$$

First two terms in the equation corresponds to the confinement energy of electron and hole respectively, third termed is associated with the columbic interaction energy and the last term defines spherically symmetrical potential well of radius "r". In the strong confinement regime the equation can be solved directly in the case of infinite spherical potential. The total

wave function (Bloch function) is expressed as product of envelope function and the function containing the periodic part of the bulk wave function. The envelope function is given by,

$$\Phi_{n,l}(r) = \left(\frac{2}{a^3}\right)^{1/2} Y_{l,m}(\theta,\Box)\ \frac{j_l(k_{n,l}\, r/a)}{j_{i+1}(k_{n,l})}$$

Where the j's are the spherical Bessel functions and Y (θ,$\Box$) is the spherical harmonic, 'l' is orbital quantum number and 'm' is azimuthal quantum number. . Here $k_{n,l}$ is the n^{th} root of the first order Bessel-function. The eigenvalues, $k_{n,l}$ are the zeroes of $j_l(k_{n,l}\, r/a)$ so that the energy levels for the electron (hole) can be expressed as the following.

$$E_{n,l}^{(e,h)} = \frac{\hbar^2 k_{n,l}^{\ 2}}{2m_{e,h}\, a^2}$$

The initial state, n = 1, l = 0, is labelled as IS and similarly next state 1P corresponds to, n = 1, l = 2. In the simple effective mass derivation of an exciton in a central potential, one can `predicts that the splitting of energy levels to be proportional to $1/a^2$ as indicated by equation 2.22. In fact the relationship is more complicated, and the extent of deviation depends on the exact band structure of the particular semiconductor in question. For very small crystallites where equation yields larger shifts, this scheme fails and one must consider non-parabolic nature of the band and the tunnelling of the electron outside the crystallite (57) In the context of effective mass potential, the relationship between band gap (the minimum energy required to excite electron from valence level to conduction level) of bulk semiconductor ($E_{g,bulk}$) and that of semiconductor nanocrystal ($E_{g,QD}$) can be expressed as,

$$E_{g,QD} \quad E_{g,bulk} + \hbar^2\pi^2/2\mu r^2$$

A more accurate expression for the band gap of quantum dot in terms of band gap of bulk semiconductor leads to,

$$E_{g,QD} = E_{g,bulk} + \frac{\hbar^2\pi^2}{2\mu r^2} - \frac{1.76}{\varepsilon_r\varepsilon_0 r} - 0.248\frac{\mu e^4}{2\hbar^2\varepsilon_r^2\varepsilon_0^2}$$

The quantization of energy on the reduction of dimensionality of the system is directly reflected in the dependence of the density of states on energy. The density of the states (DoS) of the system describes the number of states at each energy level that are available to be occupied. The density of states for a zero-dimensional system (quantum dot) has the shape of δ-peaks and mathematical given by,

$$\frac{dN}{dE} \propto \sum_{\varepsilon<E} \Theta(E-\varepsilon) = \sum_{\varepsilon} \delta(E-\varepsilon)$$

In above equation, ε is discrete energy levels, Θ is the Heaviside step function and δ is the Dirac function. Figure 2.5 gives comparable view of density of states of bulk semiconductor and semiconductor nanostructures including that of quantum dots.

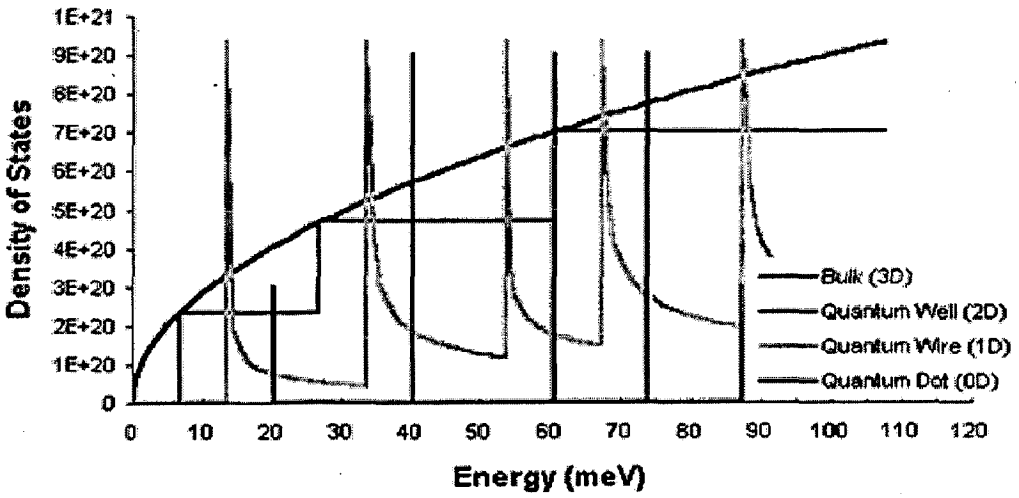

Figure 1.10 Density of states of bulk semiconductor, quantum wells, quantum wires and quantum dots.

1.5 Optical properties of quantum dots.

The energy to create electron- hole pair is can be calculated from above equations as,

$$E_{hv} = E_g + \frac{\hbar^2 K^2_{l,ll}}{2m^*_e} + \frac{\hbar^2 K^2_{l',ll'}}{2m^*_h}$$

Where E_{hv} is the photon energy, Eg is the bulk band gap and the last two terms is energy levels of electron and hole respectively. Not all states can be accessed with a single photon. In the long wavelength approximations, the oscillator strength for the absorption into a specific electron-hole pair states factors is given by,

$$f_{osc} \propto |< \Psi^e_{nlm}|\mathbf{P}|\ \Psi^h_{n'l'm'}>|^2 = |< \varphi^e_{nlm}|\ \varphi^h_{n'l'm'}>< u_c|\mathbf{P}|u_v>|^2$$

Where "**p**" is the transition dipole operator. The overlap of the electron and hole envelope function determines the strength of the transition and the unit cell transition moment take care of the usual electric dipole selection rule. The electron and hole must occupy the same space or $n = n'$, $l = l'$ and $m = m'$. There must be complete overlap of the electron and hole wave functions. The immediate consequence of the discreteness of the states and the selection rules is that the absorption spectrum should be composed of discrete bands and relatively sparse. In some crystallites the highly delocalized character of the wavefunction "s" and the close spacing between the even or "s like" and odd or "p like" wavefunction makes the states highly polarisable. As a consequence these crystallites are expected to have a large non-linear optical response.

The simplest example of this possibility is the "Stark effect" in which in the response of external electric field, the lowest "s-like" and "p-like" envelope functions should strongly mixed. This mixing results in a shift of energies and the change in the oscillation strength of the transitions.

1.6 Bioconjugation

1.6.1 General Introduction

Due to similar dimension of the nanomaterials such as nanoparticles or nanorods with those of biomolecules such as proteins (enzymes, antigens, antibodies etc.), carbohydrates, fats and nucleic acids (DNA and RNA), their conjugated systems tend to display novel properties and have unique applications. The integration of nanoparticle which exhibits unique electronic, photonic and catalytic properties with biomaterials, which displays unique recognization sites, catalytic and inhibition properties lead to new era in imaging, diagnostics and therapeutic medicine.

A variety of synthetic methodologies for the preparation of biomolecules-quantum dot conjugate within a narrow size distribution are available (59). Often these are prepared by "wet chemistry" procedures, in which clusters of semiconductor molecules are formed in the presence of a surface-capping ligand. This capping ligand binds to the semiconductor clusters, prevents aggregation of the particles into bulk material, and controls the final dimensions of the colloidal semiconductor nanocrystals. The surface capping also provides dangling bonds for further conjugation of biomolecules onto quantum dot surface and for the formation of 2-D and 3-D superstructures by means of covalent, ionic, adsorption and affinity linkage. The surface capping also helps in fine tuning the electronic and optical properties of quantum dots by surface passivation.

Biomaterials are important future building blocks for quantum dot architectures because of the several fundamental features such as:

1) Biomaterials display specific and strong complementary recognition interactions, for example, antigen-antibody, nucleic acid-DNA, and hormone-receptor interactions and hence

enable the transport of quantum dots or other nanoparticles to the inaccessible areas in human body. For e.g., Lactofferin can efficiently transport the quantum dots when conjugated to it, to the blood-brain-barrier (BBB) through lactofferin receptors in central nervous system where foreign substances experienced difficulty in penetrating that barrier.

2) Various biomolecules contain several binding sites, for e.g., antibodies exhibit two Fab (antigen-binding fragment) sites, whereas streptavidin or concanavalin A each display four binding domains. This allows the strong binding of biomolecules to the surface of quantum dots and simultaneous provides multi-functionality to the conjugate system.

3) Proteins may be genetically engineered and modified with specific anchoring groups. This facilitates their aligned binding on the quantum dots. Consequently, the directional growth of semiconductor nanocrystals structures may be dictated.

Modern efforts in biotechnology involve the application of combinatorial methods for the synthesis of new biocatalysts or drugs. The simultaneous analysis of many pathogens, mutants, insecticides, pesticides, or therapeutic drugs is a major challenge in bioanalytical chemistry. Thus, the unique optical or electronic properties of semiconductor nanoparticles are of key interest for the development of high-throughput techniques for the parallel analysis of numerous components in samples. The possibility to control and tune these unique optical and electronic properties of semiconductor nanoparticles through their dimensions paves the way for their as versatile analytical probes and multi-colour imaging. The importance of functionalized nanoparticles for biomedical applications cannot be overestimated. For instance, targeted entry into cells is an increasingly important area of research (57).The nucleus is a desirable target because the genetic information of the cell and transcription

machinery resides there. Targeted nuclear delivery is a challenging task because a nuclear probe must, at least, satisfy the following requirements:

1) It should enter the cell (e.g. through receptor-mediated endocytosis),

2) It should escape endosomal/lysosomal pathways,

3) It should possess a nucleus localization signal to interact with the nuclear-core complex, and

4) The probe should be small enough (< 30 nm) to cross the nuclear membrane.

1.6.2 Synthesis of biomolecule-conjugated quantum dots

Biological molecules have been immobilized on quantum dots by variety of techniques that includes physical adsorption, electrostatic binding, specific recognition, and covalent coupling (58, 59). These nanoparticles, which are modified with biological molecules such as proteins/enzymes, antigens/antibodies, and DNA/oligonucleotides, have been used for numerous biotechnological applications: affinity separations, biosensing, bioimaging and drug delivery. Figure 1.11 shows outline for the generation of bio-nanomaterial to yield functional devices.

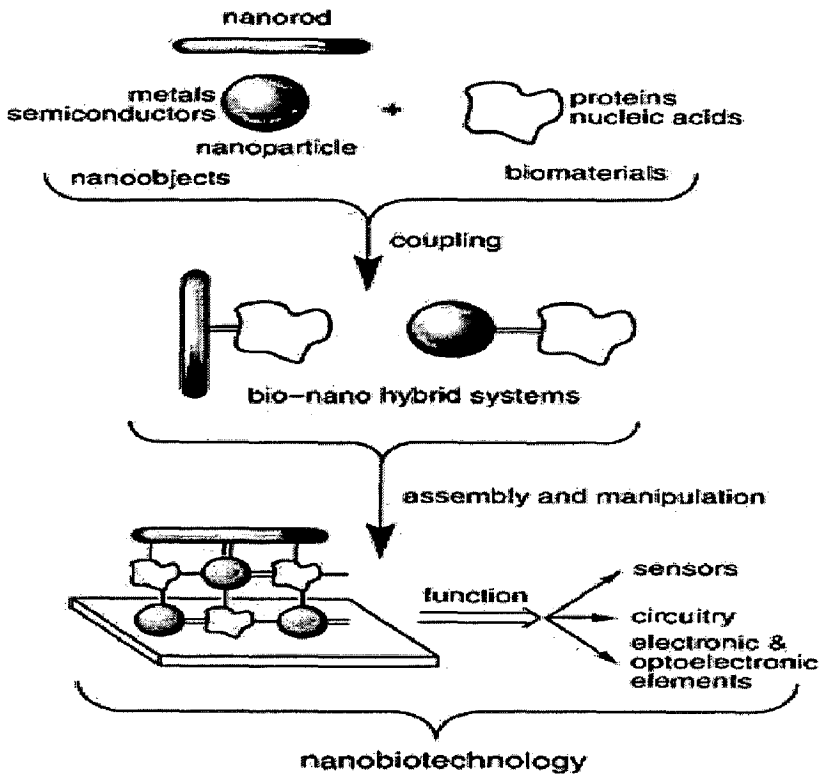

Figure 1.11 The conceptual generation of biomolecule-nanoparticle/nanorod conjugates to yield functional devices.

Chapter 2

2. LITERATURE REVIEW

2.1 Synthesis and Characterization of II–VI Nanoparticles

The field of ''synthesis'' or ''preparation'' of II–VI semiconductor nanoparticles has experienced an enormous development in the past two decades. The literature dealing with this topic is virtually unmanageable. Even the shortest history of the preparation of II–VI semiconductor nanoparticles has to start with the work published by A. Henglein in 1982 (60). Like others, this paper deals with surface chemistry, photodegradation, and catalytic processes in colloidal semiconductor particles. But it is this very work which reveals the first absorption spectrum of a colloidal solution of size-quantized CdS nanocrystals. These were prepared from $Cd(ClO_4)_2$ and Na_2S on the surface of commercial silica particles. Another milestone in the preparation of II–VI semiconductor nanocrystals is the work by Murray, Norris and Bawendi from 1993 (61) Their synthesis is based on the pyrolysis of organometallic reagents like dimethyl cadmium and trioctylphosphine selenide after injection into a hot coordinating solvent. This approach provides temporally discrete nucleation and permits a controlled growth of the nanocrystals. Rossetti et al. reported on quantum size effects in the redox potentials and electronic spectra of CdS nanocrystals (62) Resonance Raman spectra were taken from freshly prepared samples and from larger, ''aged'' particles. The size distributions were studied with transmission electron microscopy (TEM), and the crystallinity and crystal structure were determined.

CdS sols with particles ranging in size between 4 and 6 nm were prepared by first precipitating Cd^{2+} ions with the stoichiometric amount of injected H_2S followed by an ''activation'' of the colloid by addition of NaOH and excess Cd^{2+} ions, resulting in a strong emission band close to the energy of the band edge.

The nature of the stabilizer plays an important role in the efficiency of luminescence quenching as demonstrated by the comparison of inverse micelle/HMP and thiophenol-capped CdS (63). Thiol capping is also the clue to synthesizing differently-sized CdTe particles prepared in aqueous solution (64) In this interesting paper, the bandgaps of 2.0 nm, 2.5 nm, 3.5 nm, and 4.0 nm crystallites were estimated from pulse radiolysis experiments, and their dependence on the size of the particles was found to be in better agreement with pseudopotential (65) and tight-binding models (66, 67) than with the effective mass approximation (68).

2.2 Thiol-Stabilized Nanoparticles

Herron et al. (69) reported on the synthesis and optical properties of a cluster with a 1.5 nm CdS core having the total formula $[Cd_{32}S_{14}(SPh)_{36}]$. 4 DMF (SPh ¼ thiophenol, DMF ¼ N, N-dimethylformamide). Its structure, being a piece of the cubic lattice as determined by single crystal XRD. The same preparative approach, i.e. the dissolution of a metal salt in water in the presence of a stabilizing thiol, yields nanocrystals of CdSe (70)], CdTe (71-73), HgTe (74) and CdHgTe (75) The thiols used were 1-thioglycerol, 2-mercaptoethanol, 1-mercapto-2-propanol, 1,2-dimercapto-3-propanol, thioglycolic acid, thiolactic acid, and cysteamine (76). The interaction of γ-radiation with Cd_{2+} and thiol-containing sols yields small CdS particles, with the dose of the radiation determining the size of the evolving particles (77). In a recent report, Gaponik et al. stress the advantages of thiol-capping of CdTe as an alternative to organometallic preparation routes (78). This article reports mean

Cd-S distances of thiol- and phosphatestabilized CdS nanocrystals determined by EXAFS at 5 K as a function of the particle diameter (79,80) Synthesis and Characterizations the aqueous synthesis, the structure, some optical properties, and the process ability of thiol-capped CdTe nanocrystals, with an emphasis on the procedures, leading to highly luminescent particles having room temperature quantum efficiencies of up to 40%. The advantages and disadvantages of different thiols used as capping agents of CdTe QDs which are relevant for the further design of surface properties of the nanocrystals are discussed.

2.3 Lactoferrin

Lactoferrin (Lf) is a mammalian cationic iron-binding glycoprotein belonging to the transferrin family which was discovered 70 years ago, and isolated simultaneously from human and bovine milks in 1960. It is widely distributed in all biological fluids and is also expressed by immune cells, which release it under stimulation by pathogens. Lactoferrin is a glycoprotein with a molecular weight of about 80 kDa, which shows high affinity for iron. The molecular structure and amino acid sequence of human lactoferrin were discovered in 1984. Lactoferrin was then classified as a member of the transferrin family, due to its 60% sequence identity with serum transferrin .

Three different isoforms of lactoferrin have been isolated. Lactoferrin-α is the iron binding form, but has no ribonuclease activity. On the other hand lactoferrin-β and lactoferrin-γ demonstrate ribonuclease activity but they are not able to bind iron. Lactoferrin is comprised of a single polypeptide chain containing 703 amino acids folded into two globular lobes. These lobes, also called C – (carboxy) and N – (amino) terminal regions, are connected with α-helix. Each lobe consists of two domains known as C1, C2, N1, and N2. The domains create one iron binding site on each lobe.

2:4 Cross linking.

Cross-linking to carboxyl groups is mediated by a water-soluble carbodiimide. Carbodiimides effect conjugation of carboxyl to primary amines or hydrazides and result in formation of amide or hydrazone bonds. The conjugation is performed between pH4.5 to 7.5; however, reaction conditions of pH4.5-5.0 are generally recommended. The reaction takes only a few minutes to complete. The carboxyl termini of proteins, glutamic acid and aspartic acid side chain are targets. Since there is an abundance of both carboxyl and primary amine groups in protein, in the presence of excess of carbodiimides, polymerization may occur. Since there is no spacer between the reacting groups, carbodiimides are called zero spacer arm cross-linkers and the resulting bond is the same as a peptide bond. Carbodiimides react and activate the carboxy acid groups to form an active intermediate (O-acylisourea). This intermediate reacts with a primary amine to form an amide derivative.

The O-acylisourea intermediate is unstable in aqueous medium and the failure to react with amine results in hydrolysis and formation of an N- reaction and is dependent on temperature, pH, and bufer composition. Tris, glycine, unsubstituted urea and regeneration of the carboxylic groups. The hydrolysis of carbodiimide is a competing and acetate buffers are not recommended. Phosphate bufers reduce coupling efciency, which can be compensated by increasing the concentration of carbodiimides.

Chapter 3

3.Materials and Methods

3.1 Chemicals and Reagents

For synthesis of cadmium sulphide (CdS) nanocrystals, cadmium chloride dihydrate ($CdCl_2.2H_2O$), thiourea, and sodium sulphide (Na_2S) were purchased from Merck, (Germany). Mercaptoacetic acid was purchased from HiMedia (India). For conjugation purpose lactoferrin, lysozyme and 2-(N-morpholino)ethanesulfonic acid (MES) (for MES buffer) were purchased from Sigma chemicals (U.S.A.) while 1-Ethyl-3-(3-dimethylaminopropyl)carbodiimide hydrochloride (EDC), tris(hydroxymethyl)aminomethane (Tris) (for Tris buffer), Potassium dihydrogen phosphate and potassium monohydrate phosphate (for phosphate buffer) were purchased from HiMedia. Coumarin from Fluka (Switzerland) was used as standard for quantum yields experiments. For protein estimation, Bovine serum albumin (BSA) and Folin-Ciocalteau reagent was purchased from Sigma chemicals and rest of the chemicals for protein estimation namely sodium carbonate, sodium hydroxide, copper sulphate and sodium potassium tartarate were purchased from Merck (Germany). Luria-Bertani medium from HiMedia (India) was used for growth of bacteria in growth curve experiments. All the chemicals are used as such without further purification. For washing purpose double distilled water is used. The model organism used in nanotoxicity studies was *Escherichia coli* K12 (MTCC), procured from IMTECH, Chandigarh, India.

3.2 Instruments and Equipments

The absorbance spectroscopy was done with Shimadzu-1800 U.V.-VIS spectrophotometer (Japan), fluorescence measurements were carried on RF-5301 PC Shimadzu-3500 spectrophotometer (Japan). The liquid samples were used for measurement of absorbance and fluorescence. The Infra-red (IR) spectra were recorded on NEXUS FT-IR (THERMONICOLET) by grinding sample with KBr. Zeta-potential of sample was determined from Malvern Zetasizer Nano ZS. The crystal structure and phase of the samples are determined by X-ray diffraction (XRD) using BRUKER D8 Advance diffractometer (Figure 3.1a) using Cu K_α target (λ = 1.54056 A°) radiation.

Figure 3.1 (a) BRUKER D8 Advance diffractometer,

A scan rate of 2°/min was applied to record the powder patterns in the 2θ range of 0°-90° and the average particle size were calculated by Scherrer formula ($t = 0.9 \times \lambda / \beta\ Cos\theta$), where "$t$" is the average thickness of the particle, "λ" is the X-ray wavelength, "β" is the line

broadening at half the maximum intensity (FWHM) in radians, and "θ" is the Bragg angle. Particle morphology and size were characterized by Field Emission Scanning Electron Microscope (FE-SEM) on FEI- TECNAI-G_2 scanning electron microscope (Fig., 3.2b). The Image of quantum dots incubated with *Escherichia coli* was recorded on fluorescence microscope ((Leica, 020-519).

Figure 3.21(b) FEI- TECNAI-G_2 scanning electron microscope

3.3 Synthesis of cadmium sulphide (CdS) quantum dots

The CdS quantum dots are synthesized by arrested–precipitation method as follows: 25 mL of 0.01M of cadmium chloride dihydrate was dissolved in distilled water in 200 mL glass beaker .To this 2-mercaptoacetic acid was added dropwise with continuous stirring till pH of the solution drops to 2. The reaction mixture was stirred for 10 min. Thereafter 25 mL 0.05 M of aqueous solution of thiourea was added to the beaker containing reaction mixture and stirred for 15 minutes. The pH of reaction mixture was adjusted using sodium hydroxide solution followed by addition of 25 mL aqueous solution of sodium sulphide dropwise. The

reaction mixture was stirred for 1 h to obtained light yellow solution. The resultant solution was centrifuged to 20,000 rpm for 1 h to obtained sedimented nanocrystals.

3.4 Derivitization of CdS quantum dots with lactoferrin and lysozyme.

Lactoferrin and lysozyme were coupled covalently at the nanocrystal surface by using1-Ethyl-3-(3-dimethylaminopropyl) carbodiimide hydrochloride (EDC) as coupling reagent. Ten milligrams of CdS quantum dots were suspended in 5 mL MES buffer (pH 5.5) with stirring. To this solution, 10 mg of EDC was added with shaking for 1 minute. Finally, 5 mL of the protein, lactoferrin or lysozyme (2 mg/mL) in MES buffer (pH 5.5) was added to the solution and mixed gently overnight at the room temperature. The solution was then centrifuged for 40 min at 20,000 rpm. The supernatant was used for protein estimation. The conjugation of protein on quantum dot was investigated by observing peaks in FT-IR spectra. The amount of protein coupled was determined using Lowry's method by calculating the difference between the total amount of protein added and the amount present in the supernatant.

3.5 Protein estimation by Lowry method

The analytical reagent for protein estimation was made as followed,

(a) 50 ml of 2% sodium carbonate solution was mixed with 50 mL of 0.1 N NaOH solutions (0.4 gm in 100 mL distilled water.)

(b) 10 mL of 1.56% copper sulphate solution was mixed with 10 ml of 2.37% sodium potassium tartarate solution.The analytical reagent was then prepared by mixing of 2 mL of (b) with 100 mL of (a).

Freshly prepared solution of Folin-Ciocalteau reagent was prepared by diluting it with equal volume of water (2 ml of commercial reagent + 2 ml distilled water).

Procedure

1. Different dilutions of BSA solutions were prepared by mixing stock BSA solution (1 mg/ ml) and water. The final volume in each of the test tubes was 5 mL. The BSA range of different dilutions was 0.05 to 1 mg/ mL.

2. From these different dilutions, 0.2 mL protein solution was pipetted to different test tubes and followed by addition of 2 mL of analytical reagent. The solutions were mixed well by vortexing.

3. The solution was incubated at room temperature for 10 min.

4. Then 0.2 ml of reagent Folin Ciocalteau solution (reagent solutions) was added to each tube and incubated for 30 min. The optical density of solutions was taken at 660 nm.

5. The graph was then plotted between absorbance against protein concentration to get a standard calibration curve.

6. Absorbance of unknown sample was determined at 660 nm and the concentration of the unknown sample was determined by using standard curve.

3.6 Growth curve of bacteria Escherichia coli K12 and nanotoxicity studies of bare CdS quantum dots and conjugated quantum dots.

3.6.1 Preparation of media:

3.6.1.1 Liquid media (Luria-bertani (LB) Broth)

The liquid media was prepared by dissolving 2.5 g of LB broth in 100 mL of distilled water in a 500 mL of Erlenmeyer conical flask (Final pH is 7.5). Flasks were autoclaved at a pressure of 15 lb/in^2 at 121 °C for 15 min.

3.6.1.2 Solid media (MacConkey agar)

Solid media was prepared by dissolving of a MacConkey agar in 100 mL of double distilled water in a 500 mL Erlenmeyer flask. It was then autoclaved at a pressure of 15 lb/in^2, 121 °C for 15 min. It was poured in to Petri dishes and allowed to solidify in laminar air flow hood for the maintenance of the sterile conditions.

3.7.1.3 Bacterial growth experiment

The culture of *E.coli* K-12 was growth overnight at 37 °C and 200 rpm shaking in liquid medium. From then, it was streaked to MacConkey agar plates in order to ascertain the purity of the culture. A single colony was picked up from agar plate and inoculated in a 100 mL of LB broth kept at 37 °C and 200 rpm. The cultures were allowed to grown till optical density at the wavelength of 600 nm (A_{600}) reached to 0.6 (25 µL of media contained $2 * 10^7$ cells at this stage). This culture was then subcultured into fresh liquid medium with different amount of quantum dots (bare as well as bioconjugated) and was allowed to grow at 37 °C and 200 rpm. The turbidity of the flask was continuously monitored at A_{600} for 15-18 h. Then the growth curved was plotted between optical density against time (in hours).

Chapter 4

4. RESULTS AND DISCUSSION

4.1 Synthesis of cadmium sulphide (CdS) quantum dots

Figure 4.1 shows images of synthesized CdS quantum dots. These images were taken under U.V lamp operating at 354 nm and images so obtained clearly showed fluorescence emission of prepared quantum dots. It can be inferred from the images that size of synthesized CdS quantum dots should be comparable to the Bohr exciton radius which in the case of CdS is 5.5 nm. The emission of different fluorescence colours indicates that they are of different sizes.

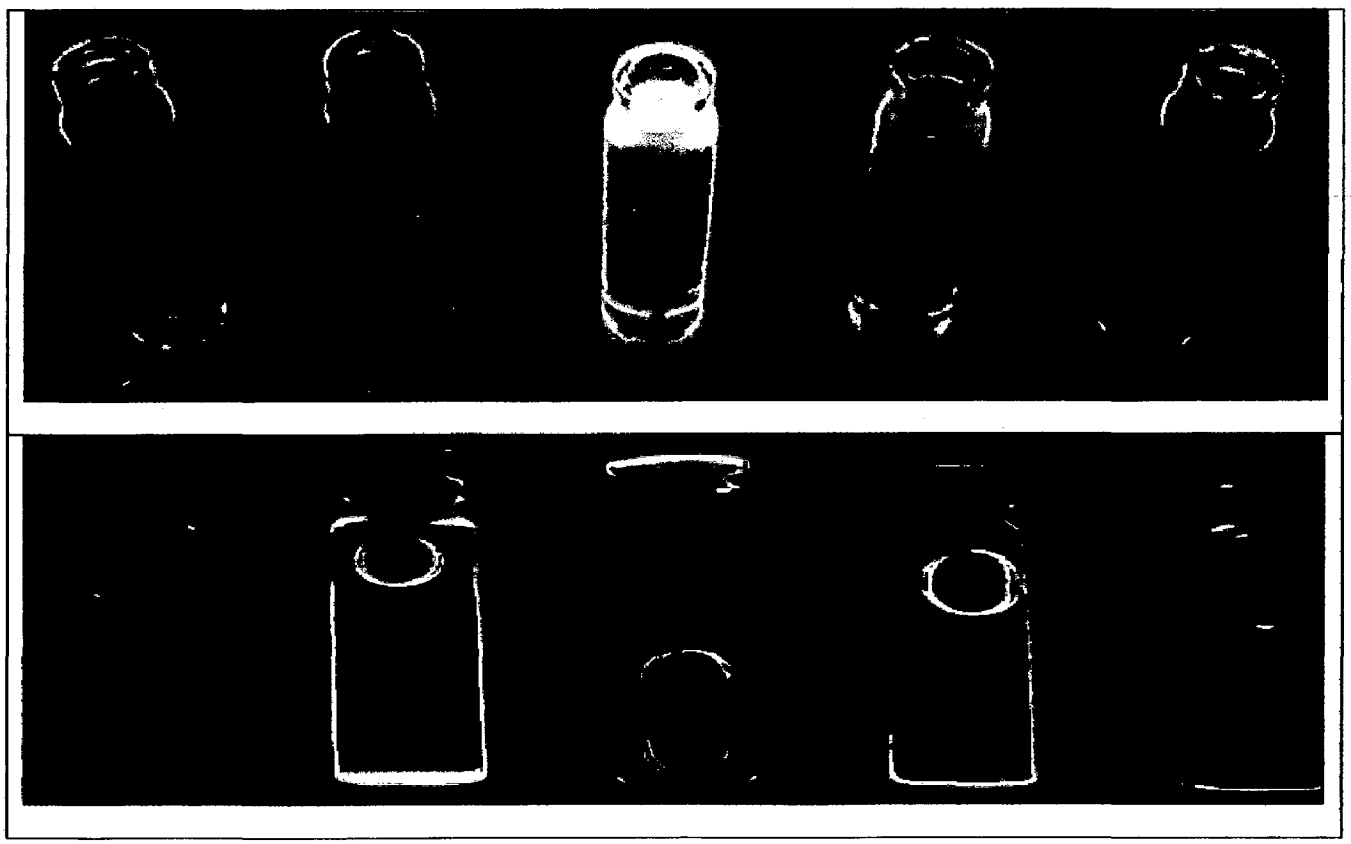

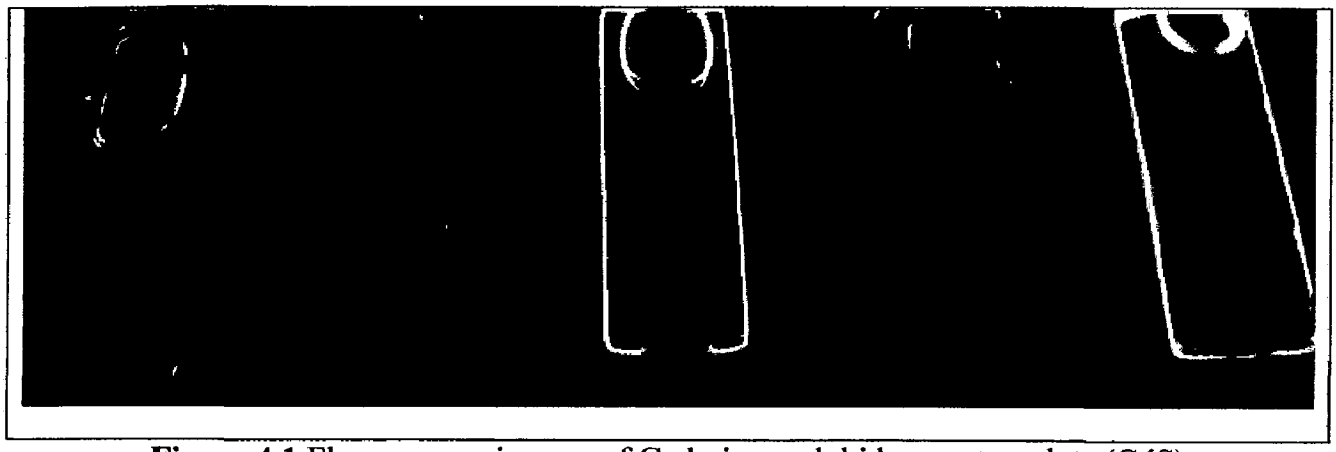

Figure 4.1 Fluorescence images of Cadmium sulphide quantum dots (CdS)

4.2 Optical properties of CdS quantum dots

4.2.1 UV-VIS Spectroscopy

The U.V absorption spectrum of quantum dots prepared in different pH of reaction mixture is shown in Figure. 4.2. There is characteristics blue shift in all samples as compared to bulk sample. The observed blue-shift is due to quantum confinement effect.

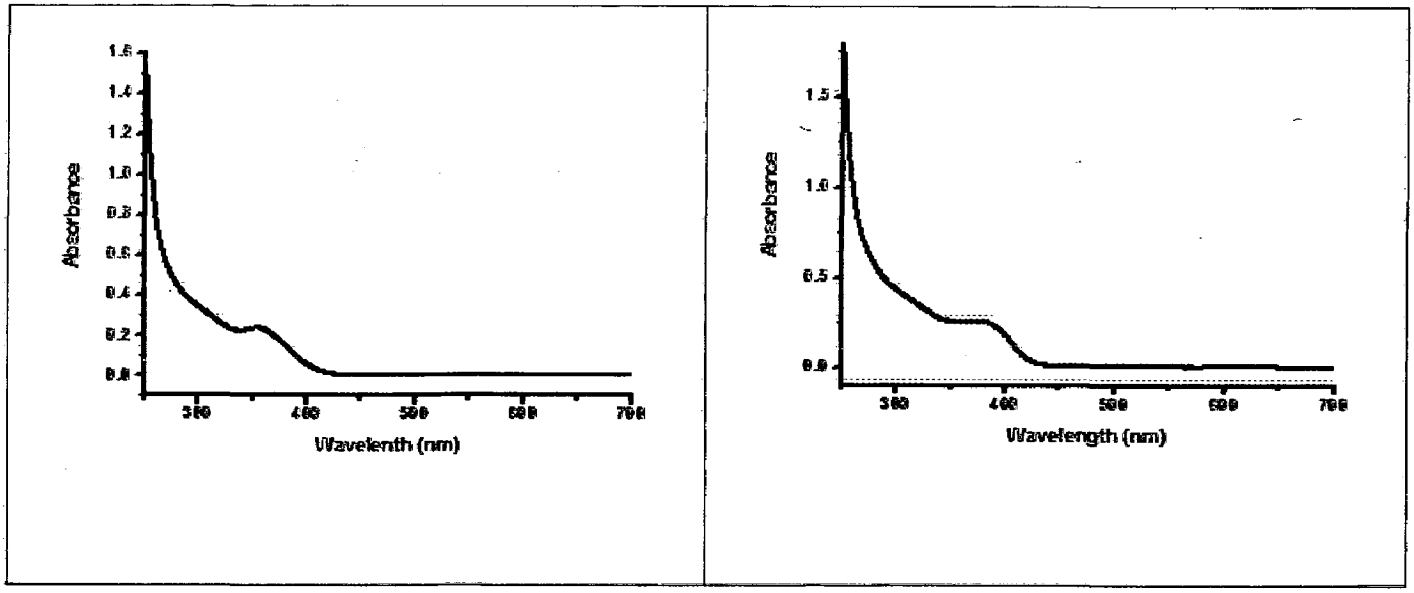

(a) (b)

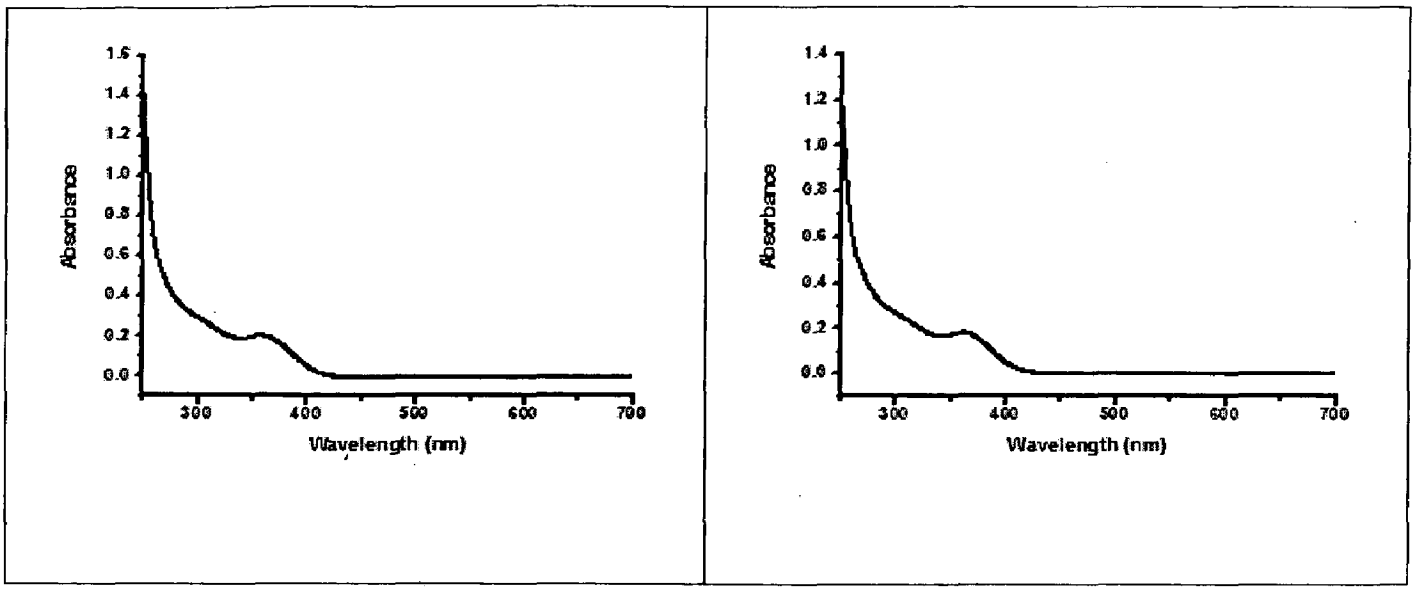

Figure 4.2.1 Absorption spectra of series of CdS quantum dots: (a) 0.01 M, pH 5.0 (b) 0.01 M pH 6.0 (c) 0.01M pH 7.0 and (d) 0.01 M pH 8.0

The band gap of bulk CdS is 2.42 eV (512 nm). We also calculated the band gap of synthesize nanocrystals under the approximation of effective mass model by taking electron effective mass (m^*_e), hole effective mass (m^*_h), and dielectric constant for CdS as 0.19 m_o, 0.8 m_o, and 5.7 in equation given below (m_o being rest mass of electron),

$$E_{g,QD} \quad E_{g,bulk} + \hbar^2\pi^2/(2\mu r^2)$$

Where "μ" is reduced mass of the electron-hole system and given by,

$$\mu = \frac{m_e^* m_h^*}{m_e^* + m_h^*}$$

and $E_{g,QD}$ is calculated by the expression $E_{g,QD} = hc/\lambda$, λ being wavelength of the absorption edge of the quantum dots and can be determined from the absorption spectrum of

the quantum dots. The radius of quantum dots as calculated from above formula is given in Table 4.2.1.

The absorption maxima of all samples found to be between 320 nm and 380 nm which is attributed to the first excitonic peak $1s_h$-$1s_e$ transition. Other high level transitions occur at much lower wavelength and difficult to observe due to size induced broadening of spectra.

Sample	Absorption edge wavelength (nm)	Absorption maxima Wavelength (nm)	Radius (nm)
0.01M pH 5.0	460.9	354.7	2.54
0.01M pH 6.0	492.2	378.2	3.16
0.01M pH 7.0	453.16	357.1	2.63
0.01M pH 8.0	472.9	360.5	2.83

Table 4.2 Calculated radii of CdS quantum dots from effective mass approximation (EMA)

4.2.2 Fluorescence spectroscopy of synthesized quantum dots

The emission property of CdS quantum dots was examined in the range of 400 nm to 700 nm. Figure 4.2.2 shows emission characteristics of synthesized quantum dots. All of them were excited by wavelength of 350 nm. As the size of quantum dot becomes smaller, its emission shifted towards blue-end.

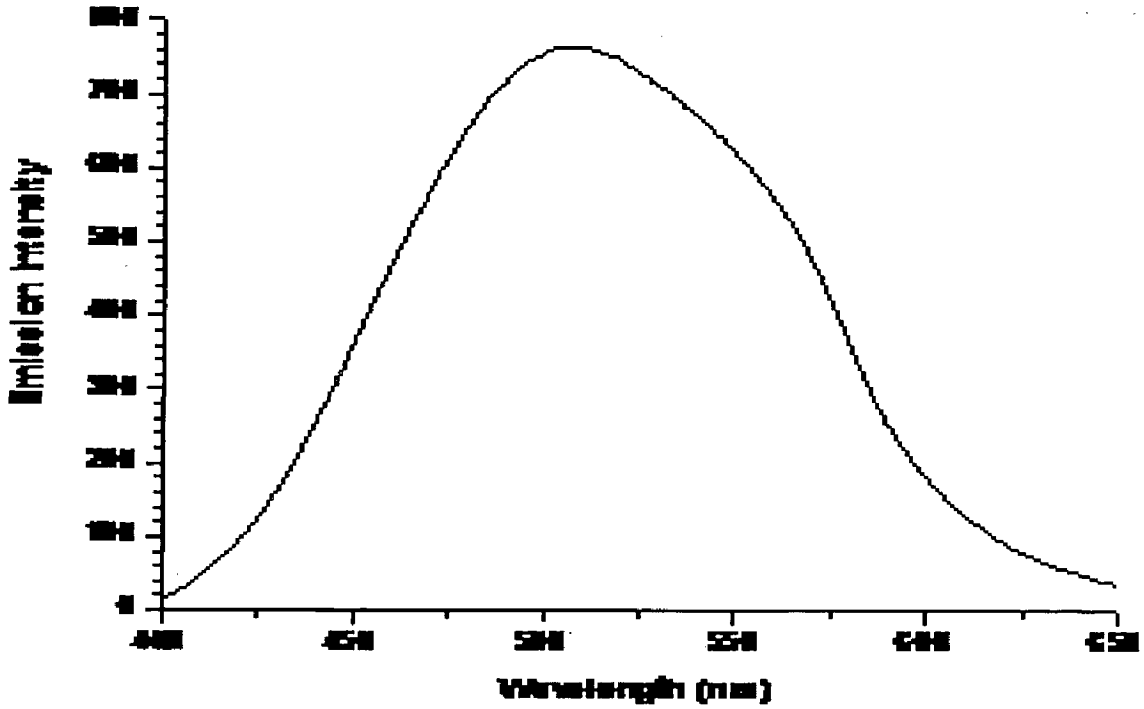

(a) 0.01M , pH 5.0

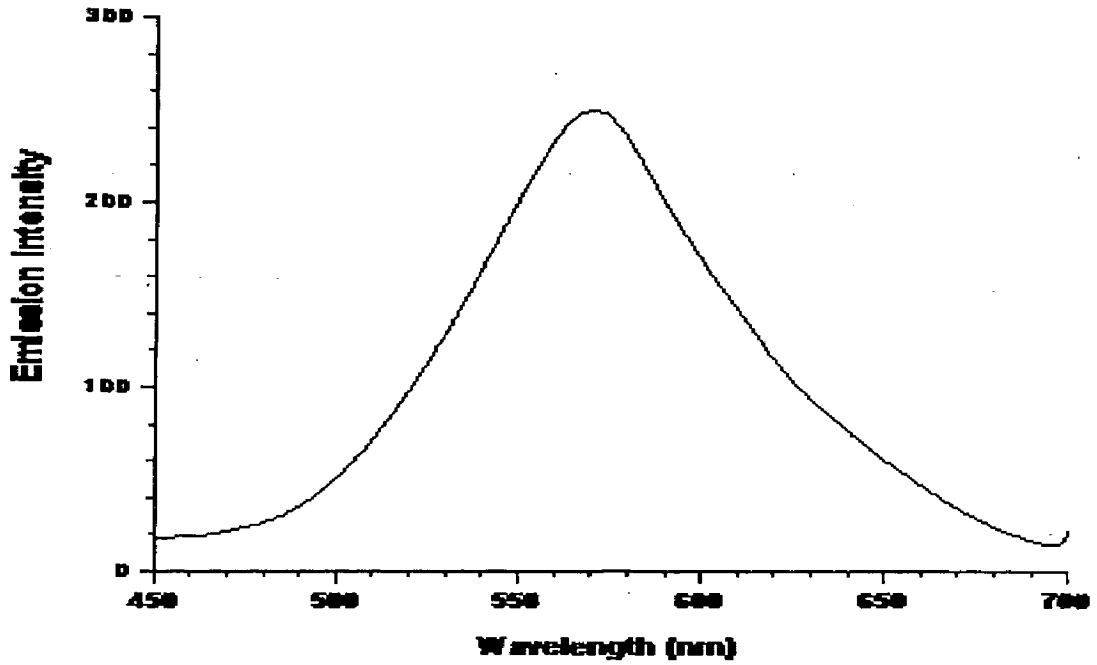

(b) 0.01 M, pH 6.0

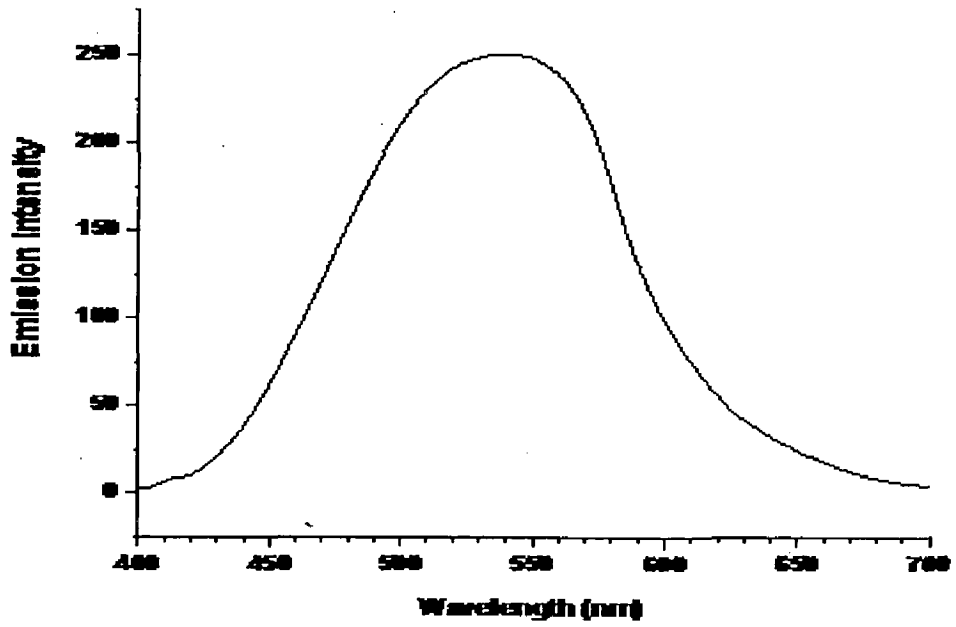

(c) 0.01M, pH 7.0

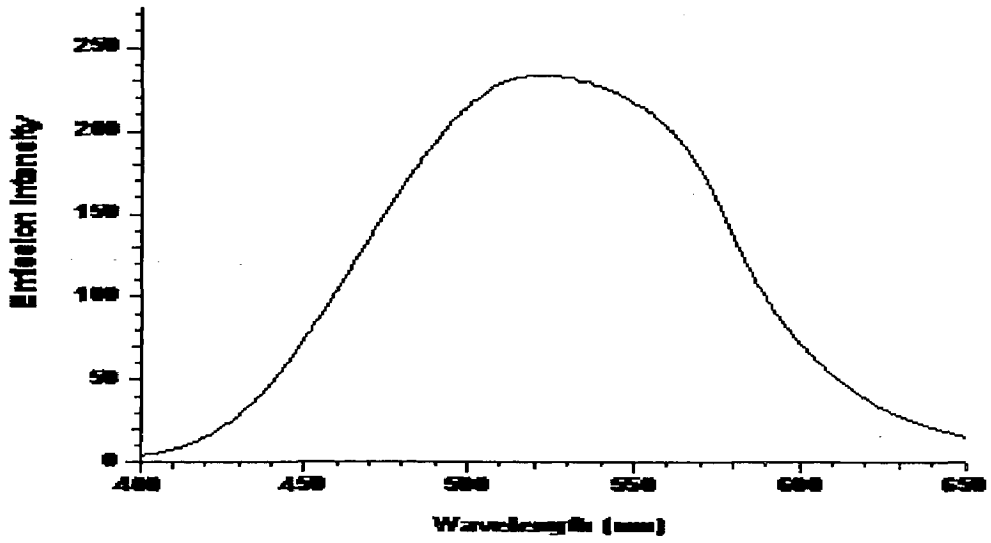

(d) 0.01M, pH 8.0

Figure 4.2.2 Emission spectra of CdS quantum dots. The emission maxima of peaks are: (a) 525 nm (b) 580 nm (c) 536 nm and (d) 528 nm.

4.2.3 Infra-red spectroscopy

The IR spectrum of synthesized quantum dot was done in order to ascertain binding of capping agent mercaptoacetic acid on the surface of CdS quantum dots (Figure 4.4). The peaks at ~3401 and ~ 1600 cm $^{-1}$ corresponds to the – OH group of the atmospheric water in KBr. The Cd-S peak was presented at 560.8 cm^{-1}. The frequencies occurring at ~1400 cm^{-1} and ~1000 cm^{-1} were assigned to C-O stretching and C-C stretching in mercaptoacetic acid (MAA) respectively. Thus FT-IR analysis reveals the presence of MAA on the surface of CdS quantum dots.

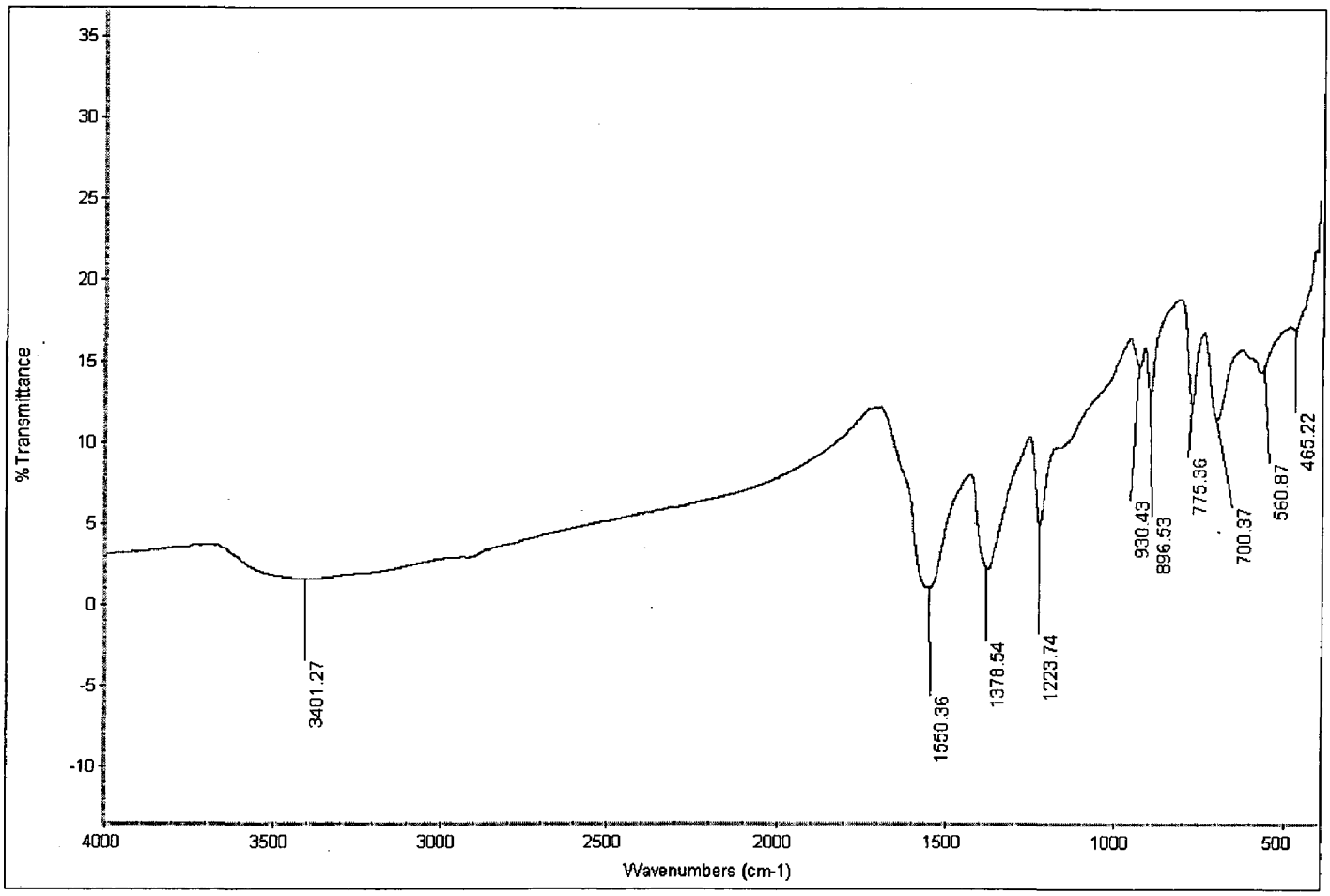

Figure 4.2.3 FT-IR Spectra showing the capping of mercaptoacetic acid on the surface of CdS quantum dot.

4.3 X-ray diffraction (XRD) pattern of synthesized nanocrystals

Figure 4.4 shows XRD pattern of CdS nanocrytals so formed. The broadening of peaks indicates that obtained crystals are in nanoregime. Furthermore, the obtained data was matched with JCPDS-file no.10-0454, which indicates that the obtained CdS are of hexagonal phase.

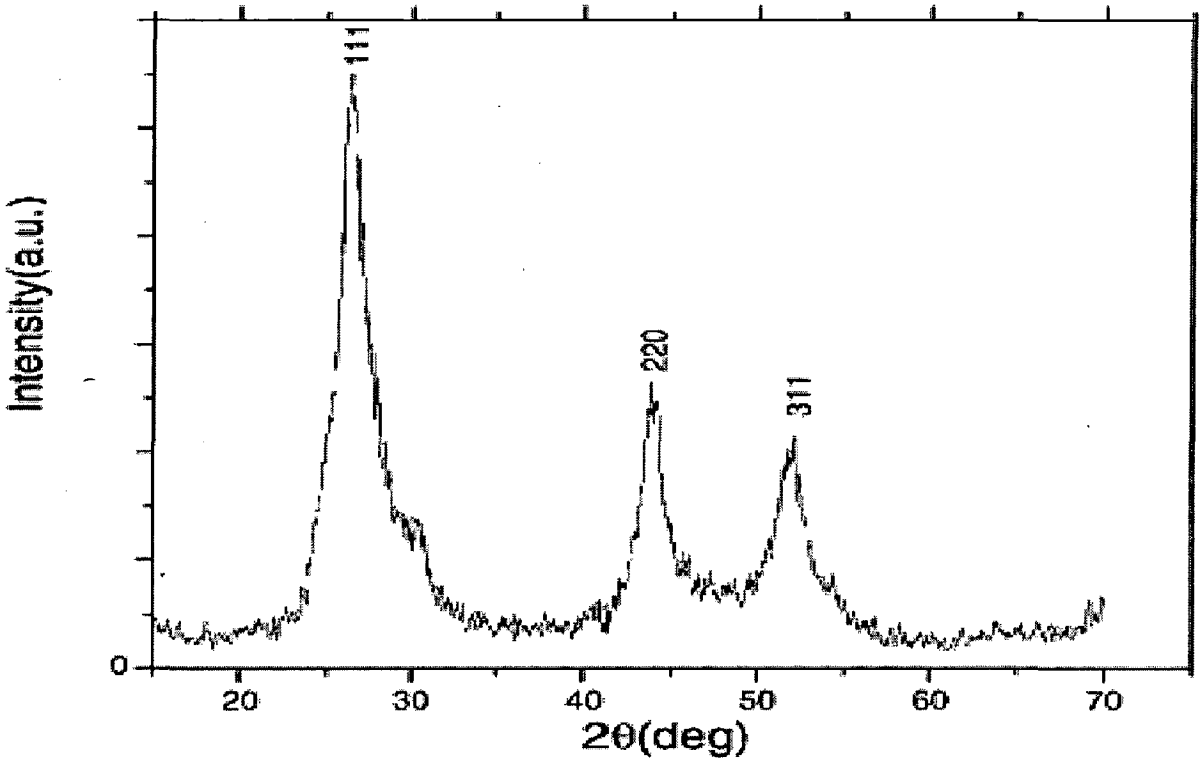

Figure 4.3 XRD-pattern of synthesized quantum dots

The particle size was calculated by using Debye-scherer formula,

$$t = \frac{0.9\lambda}{\beta \cos\theta}$$

where t is the average thickness of the particle, λ is the X-ray wavelength, β is full width at half maxima (FWHM) of maximum intensity peak in radians, and θ *is* the Bragg angle.

The average particle size as calculated from Scherer formula was found to be 8.16 nm.

4.4 FE-SEM analysis

The FE-SEM images of quantum dots are given in Figure 4.4.

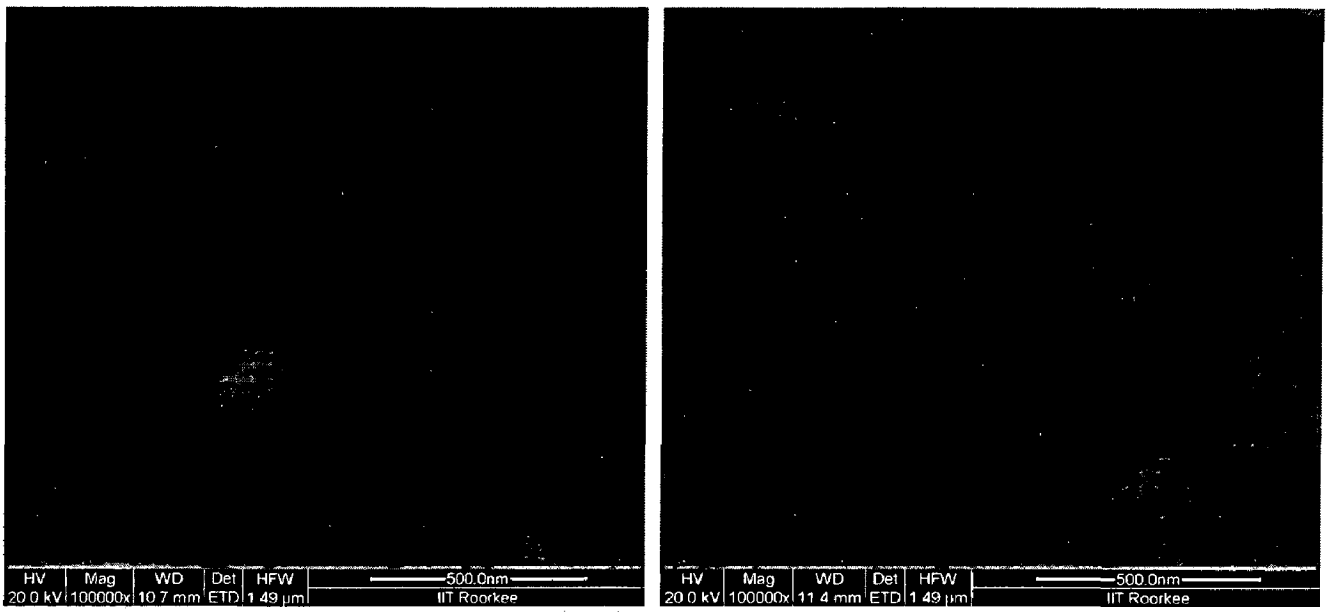

(a) **(b)**

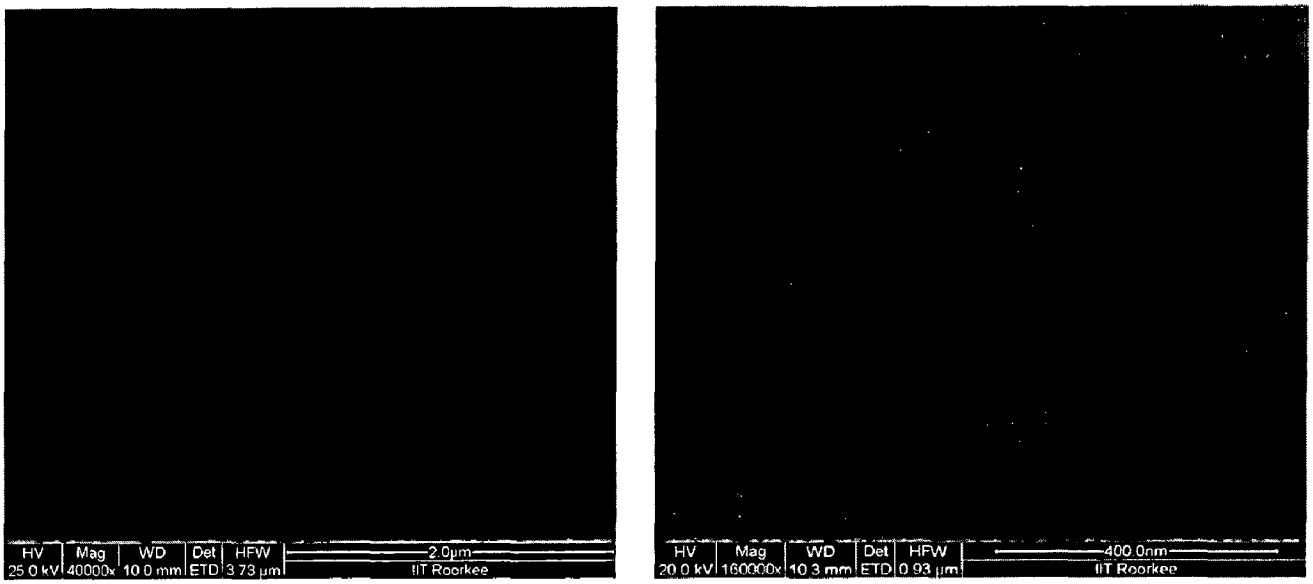

(c) **(d)**

Figure 4.4 FE-SEM images of synthesized quantum dots. Bar length (a) 500 nm, (b) 500 nm, (c) 2.0 µm and (d) 400 nm

It can be seen clearly, that the quantum dots so obtained from arrested precipitation method are nearly monodispersed and spherical in shape. Another interesting feature was seen in SEM images is the formation of leaves likes structures (Figure 4.4).

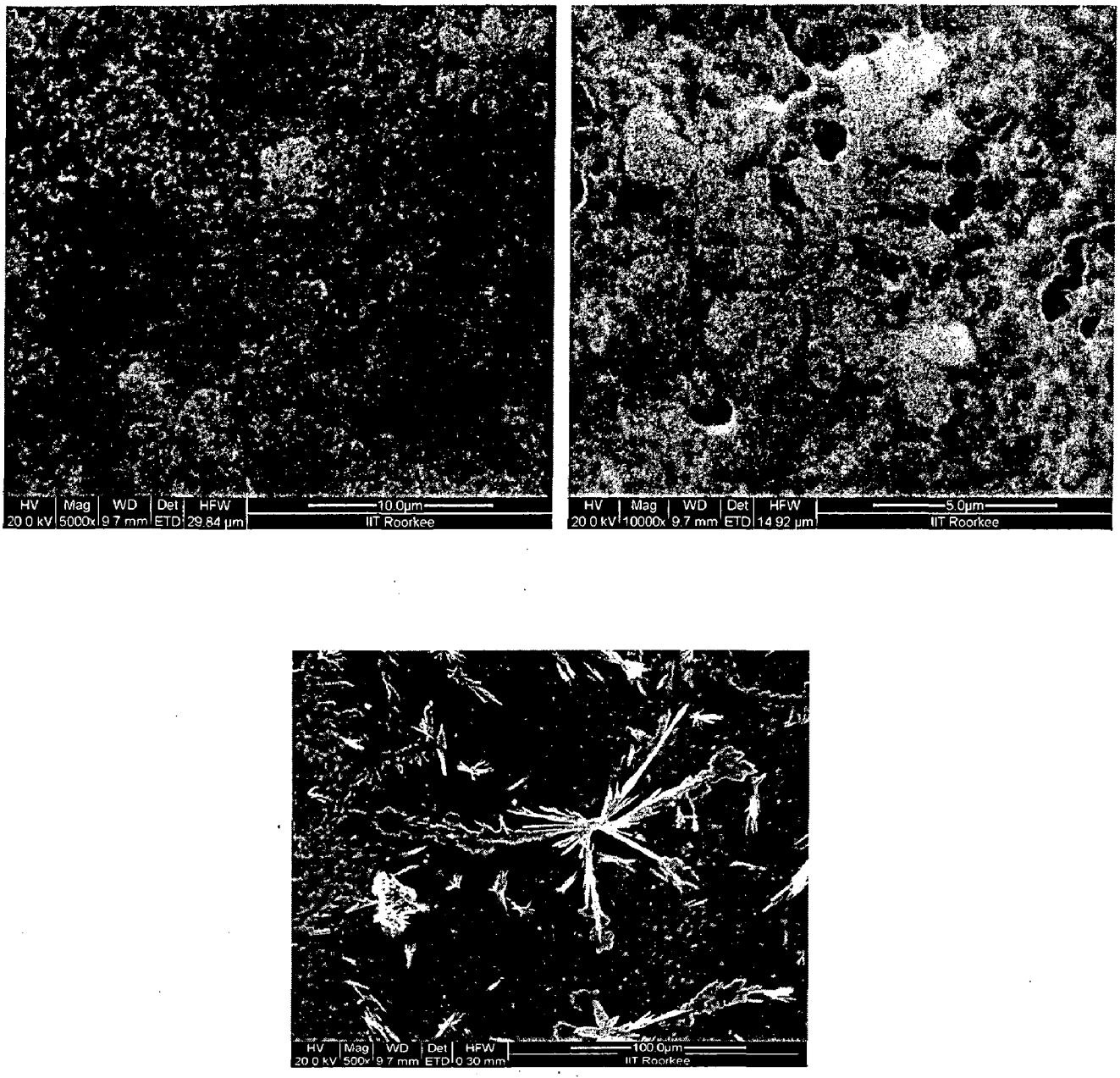

Figure 4.4 FE-SEM images of synthesized quantum dots

The possible explanation for the formation of such superstructures is due to the entanglement of side chains of mercaptoacetic acid molecules with each other. This can be due to excess of mercaptoacetic acid molecules on the surface of quantum dots. Such

structures are of interest since they can be used as sensors for detection of specific analytes due to their large surface to volume ratio.

4.5 Elemental Analysis

Element	Wt%	At%
CK	14.58	19.97
NK	01.05	01.23
OK	73.41	75.50
SK	04.61	02.37
CdL	06.93	00.93

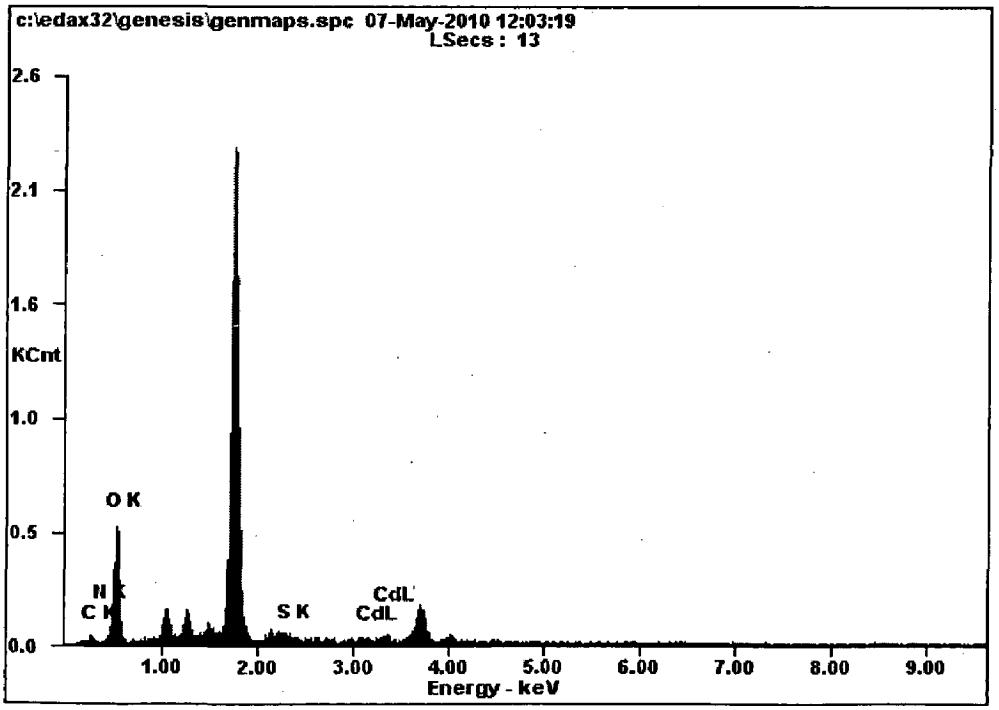

Element	Wt%	At%
CK	11.97	15.96
NK	02.81	03.21
OK	79.00	79.04
SK	02.55	01.27
CdL	03.67	00.52
Matrix	Correction	ZAF

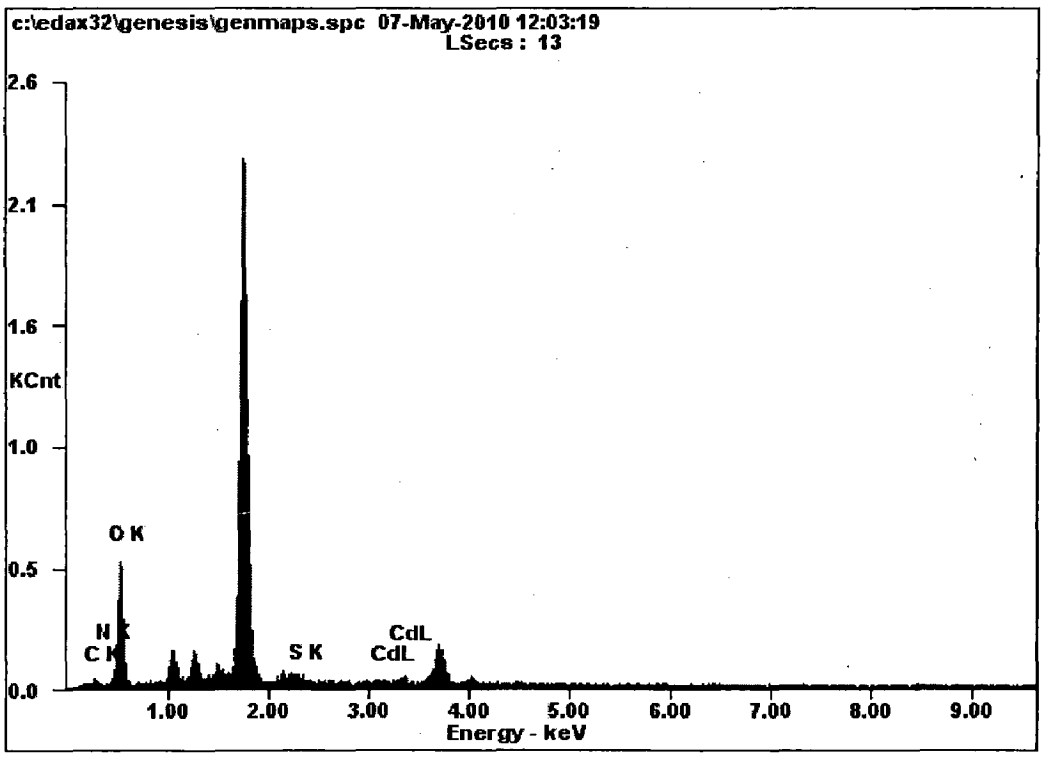

Figure 4.5 EDAX spectrum of CdS nanoparticles

From the above EDAX spectrum, it can be inferred that weight percentage of cadmium and sulphide is nearly equal. The other large peaks are due to elements of glass matrix such as silicon, magnesium, sodium etc which is used as surface on which powdered sample was applied.

The leaf–like superstructure that was formed on glass slide was believed to be due to entanglement of carboxyl acid side chains of mercaptoacetic acid with each other. This can be seen from the elemental analysis of such superstructure by means of EDAX where amount of sulphur is significantly enhanced Figure 4.8.

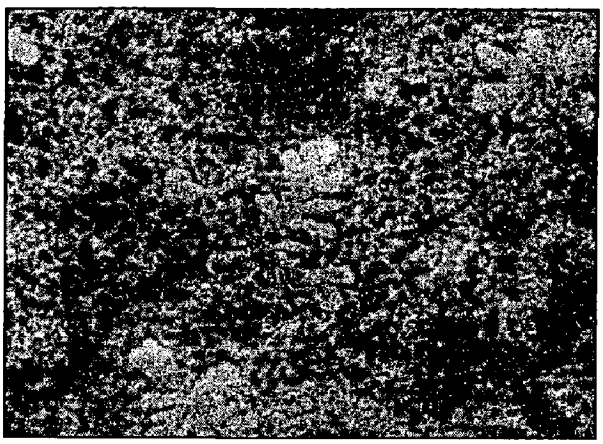

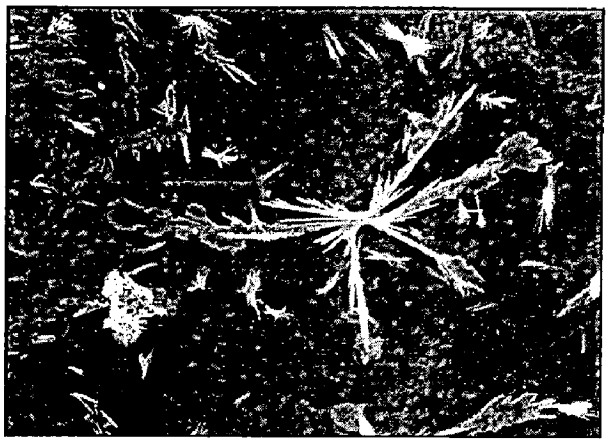

Element	Wt%	At%
CK	22.11	30.45
NK	04.87	05.75
OK	55.03	56.89
SK	11.54	05.95
CdL	06.44	00.95

Element	Wt%	At%
CK	23.78	34.79
NK	10.46	13.12
OK	38.41	42.17
SK	14.42	07.90
CdL	12.93	02.02
CK	23.78	34.79

Figure. 4.5 EDAX Spectra of leaf-like superstructure

4.6 AFM Characterization

The samples were characterized through AFM in order to get quantitative information of several parameters such as roughness, particle size distribution.

The sample preparation for AFM was done by dispersing a drop of CdS QDs on a glass slide and let it dry out completely. The Figure 4.6 gives the result of AFM analysis.

(a)

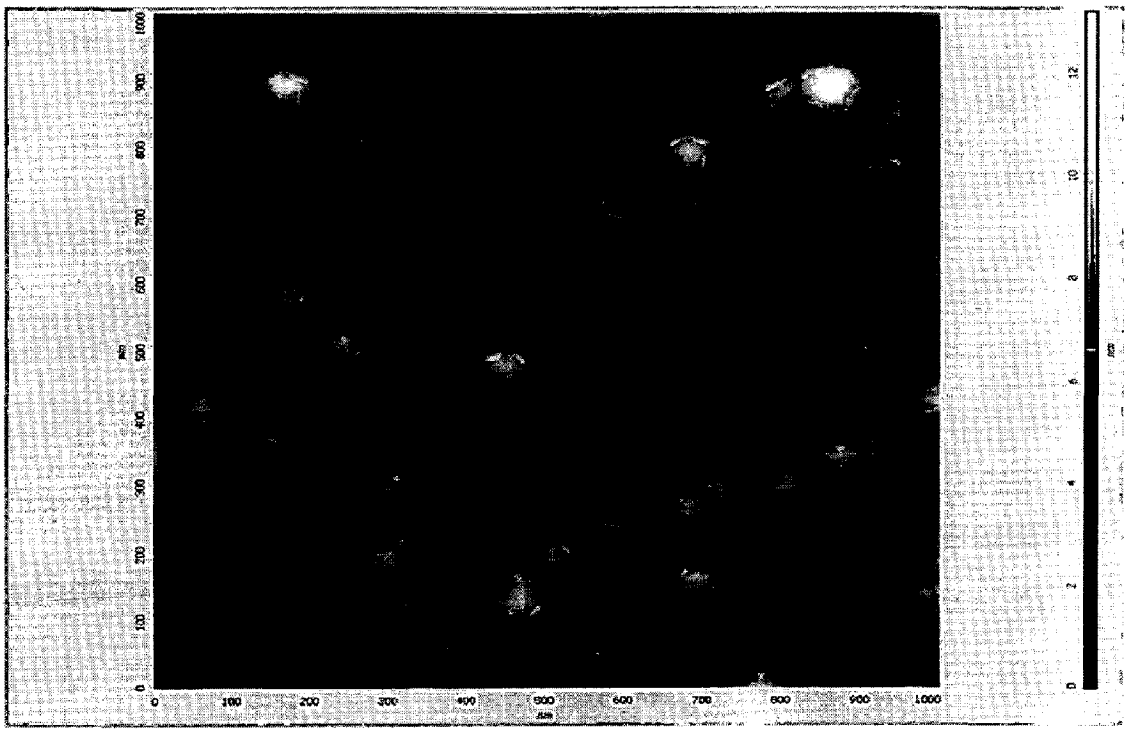

(b)

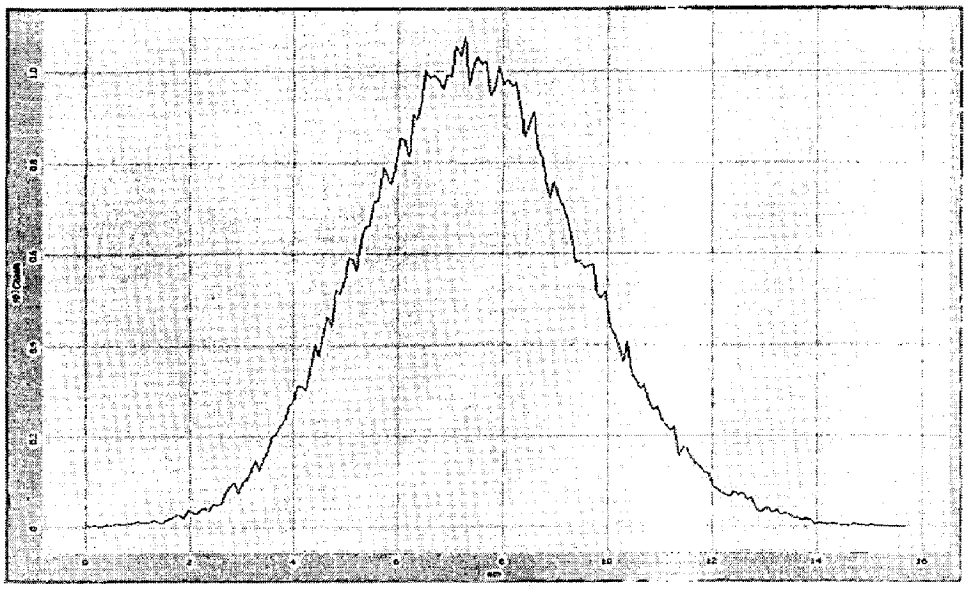

©

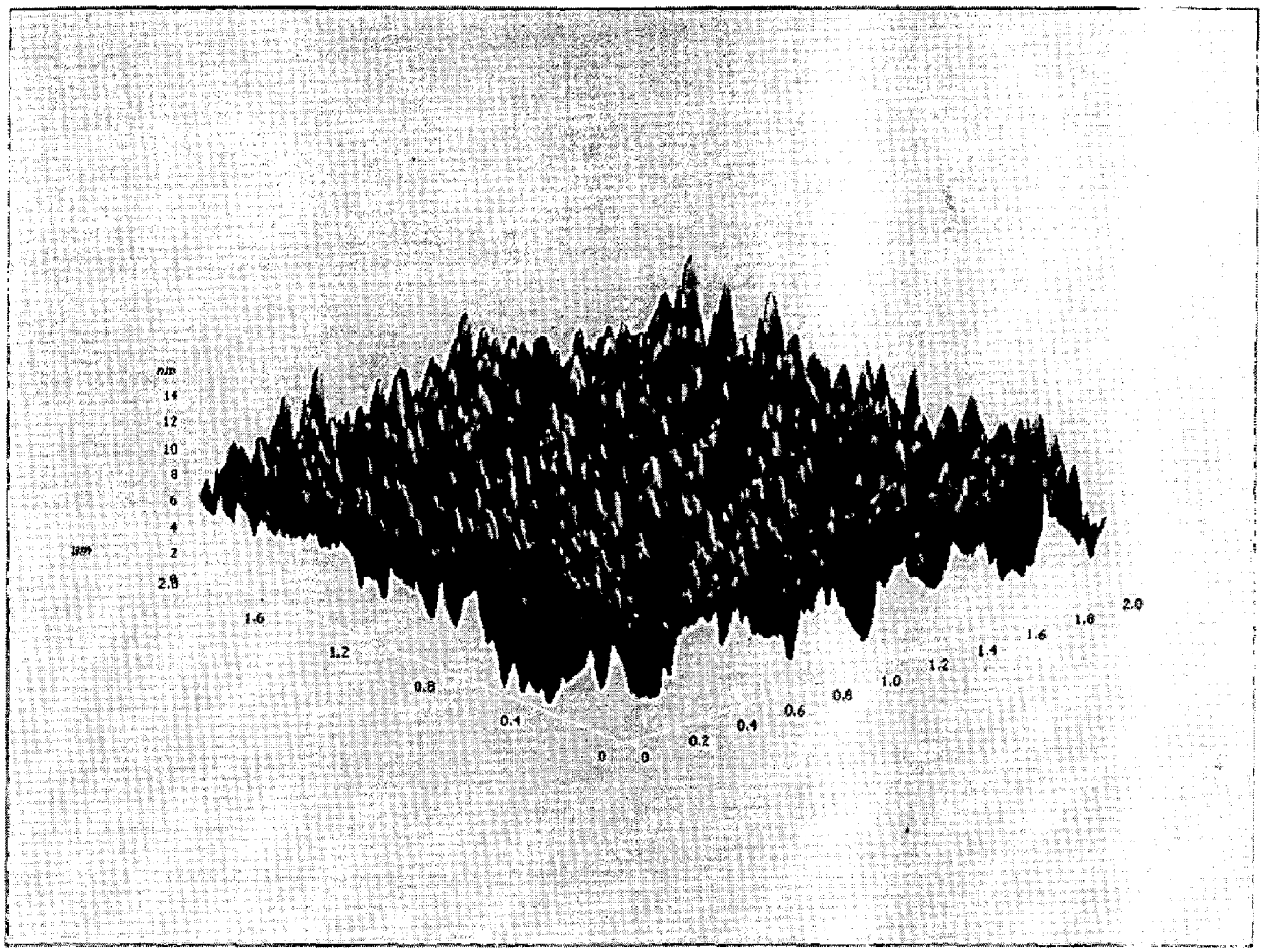

Figure 4.6 (a) AFM Image of synthesised CdS quantum dots, (b) Histogram showing the height of quantum dots, (c) 3-dimensional image

4.7 Zeta-potential studies

The surface charge of MAA capped CdS quantum dot was determined by zeta probe measurements. The sample was adequately dispersed in double distilled water by sonification. The zeta potential of CdS quantum dots was determined to be -38.8 mV (milli-volts) with standard deviation of 4.86 mV. This highly charged surface of CdS quantum dots indicates that these are very stable systems. In fact, stability of the system can be determined by considering that even after 2 months, there is insignificant change on the surface charge of the quantum dots.

4.8 Imaging of CdS quantum dots with microoraganism

One key area where applications of quantum dots are in full swing is in the field of biological imaging and molecular labelling. For this application the quantum dots must be water soluble so that they can transverse in body cells and fluids. In this study, imaging of quantum dots was done on *Candida albicans* to observe the effect of quantum dots in these organisms.

Briefly, 5 μL of metabolic active cell culture of *C. albicans* was smeared on the chick egg albumin coated glass slide followed by additions of 1μL of quantum dot solution. The mixture was allowed to incubate for 10 minutes. The glass slide was then washed with distilled water to exclude excess quantum dots and placed under the objective lens of fluorescence microscope (Leica, 020-519) fitted with camera.. The images were recorded by exciting the sample at 380 nm by placing blue filter. The images of quantum dots with cell suspension are shown in figure 4.8.

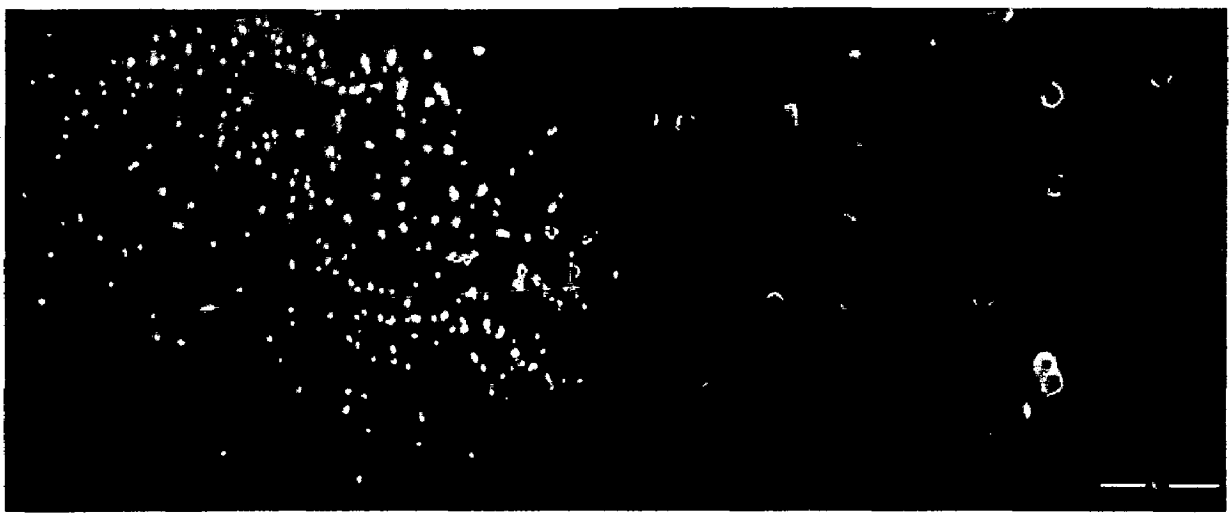

Figure 4.8 CdS quantum dots with Candida albicans.

It is clearly seen in the figure that cells seem to internalize these quantum dots into their cell membranes.

4.9 Derivitization of CdS quantum dots with lactoferrin.

In the view of role of lactoferrin as potential receptor for crossing blood-brain barrier (BBB) in the central nervous system and its therapeutic value as anti-cancer agent, it was conjugated to the CdS quantum dots. This system can be used for tracking conjugated system through blood-brain-barrier along with some drug to cure disease of central nervous system where conventional therapeutic approaches either fail or are deeply invasive and thus costly. For example, these models can act as an excellent delivery vehicle for delivering siRNA (silencing RNA) molecules with high selectivity and efficiency into tumor cells and simultaneously monitoring of both siRNA delivery and the resulting knockdown effects at the single-cell level.

Lactoferrin being protein molecule contains free amino groups. These amino groups provide excellent functionality for conjugating them to nanoparticles surface. Here, EDCI coupling chemistry was used for the conjugation of amino groups of lactoferrin with carboxyl group of mercaptoacetic acid capped CdS quantum dots.

4.9.1 Confirmation of conjugation by means of FT-IR analysis.

As shown in figure 4.11, the conjugation of lactoferrin has been proven by FT-IR spectrum. The formation of amide bond has been confirmed by observing the peak at 3400 cm^{-1}.

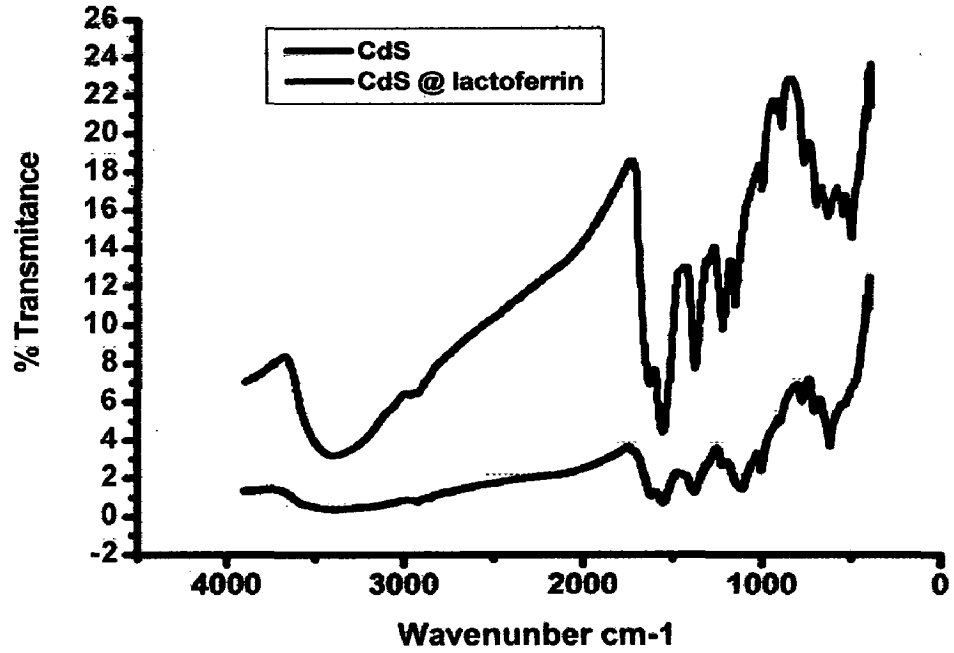

Figure 4.9.1 FT-IR spectra showing conjugation of lactoferrin on CdS quantum dots

4.9.2 Protein estimation analysis

Amount of protein bound to the quantum dot was determined by calculating the difference between the total amount of protein added and the amount present in the supernatant. The percentage of protein binding to nanoparticles by two step EDCI coupling process was found to be around 60% of the total protein added initially for binding. The numbers of lactoferrin molecules bound per particle were calculated by assuming a molecular

weight of 90 kDa for lactofferin. On average, one lactoferrin molecule was conjugated per CdS quantum dot. The solution of quantum dots functionalized with lactoferrin showed very high stability at neutral pH and no sedimentation was observed even after 15 days of storage at room temperature.

4.9.3 Optical property of lactoferrin functionalized CdS quantum dots.

(a) Absorption spectrum of lactoferrin functionalised CdS quantum dots

As can been seen from Figure 4.12, the absorption spectra of lactoferrin functionalised quantum dots is relatively red shifted. This indicates increased in size of CdS quantum dots on conjugating to the lactoferrin.

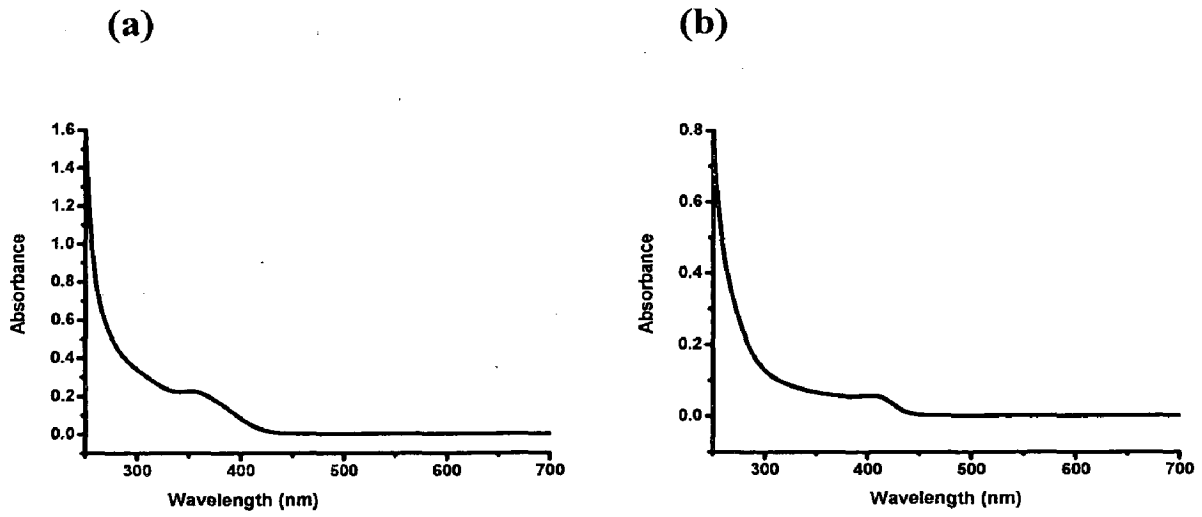

Figure 4.9.3 Absorption spectrum of CdS quantum dots (a) and lactoferrin functionalised CdS quantum dots.

Emission spectrum of lactoferrin functionalised CdS quantum dots.

The emission spectra of CdS quantum dots and lactoferrin functionalised quantum dots

are given in Figure 4.13. From the figure it can be seen that there was shift in wavelength maxima toward red end of visible spectrum for lactoferrin functionalised quantum dots relative to CdS quantum dots. There is also decrease in fluorescence intensity of lactoferrin functionalised quantum dots relative to that of CdS quantum dots.

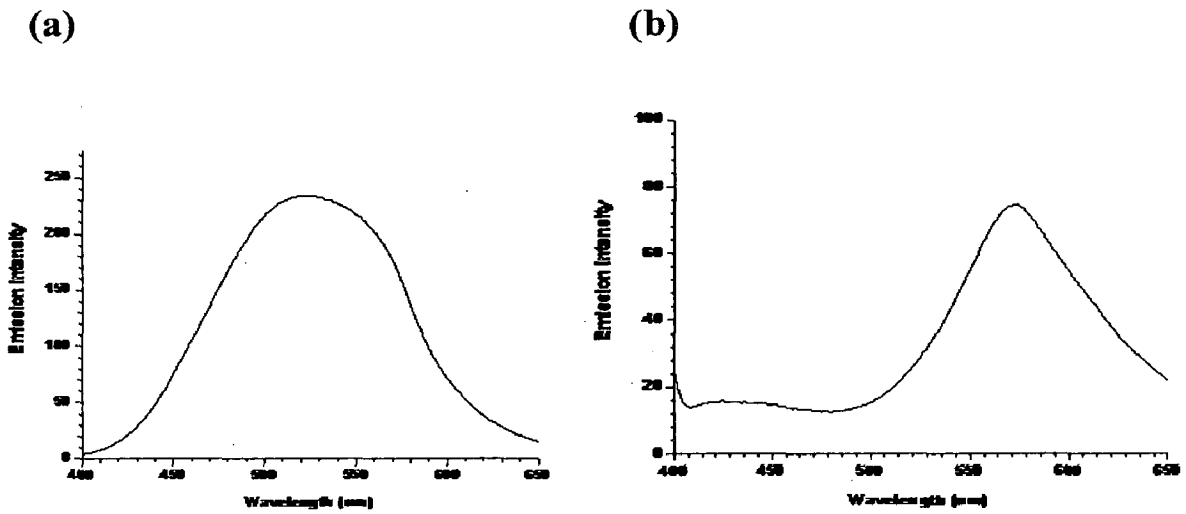

Figure 4.9.3(b) Emission spectrum CdS quantum dots (a) and lactoferrin functionalised CdS quantum dots (b)

4.11 Toxicity Studies of Lactoferrin functionalised CdS quantum Dots

The CdS quantum dots and lactoferrin functionalised quantum dots were treated with culture medium consist of *E.coli* K-12 and its toxicity was accessed in terms of growth potential of cells in the presence of these quantum dots.

As seen from Figure 4.23, the CdS quantum dots delayed the growth by nearly 10 % and corresponding delayed growth by lactoferrin functionalised quantum dots is 27% as compared to the control.

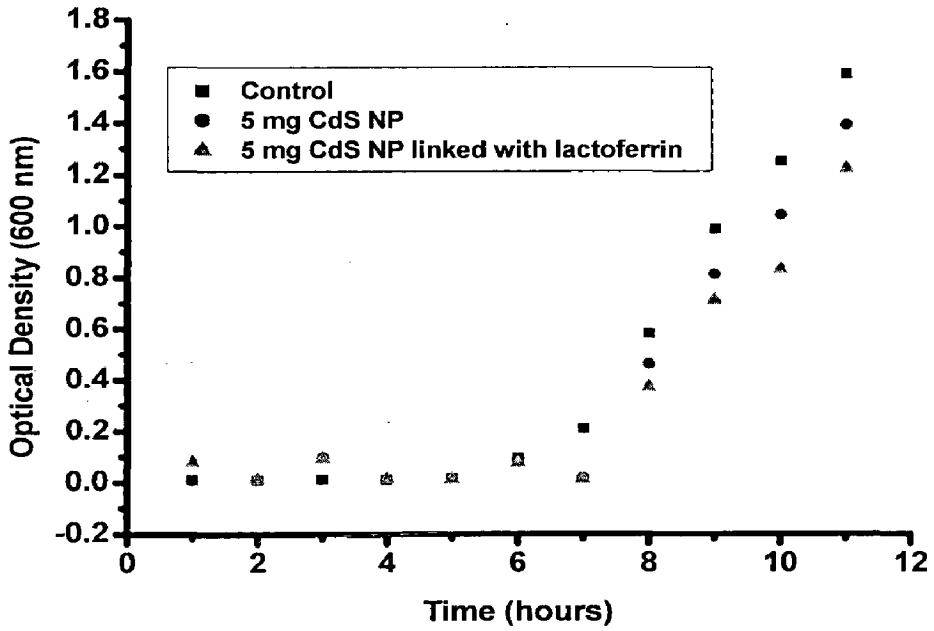

Figure 4.23 *E.coli* growth curve in the presence of CdS quantum dots and lactoferrin functionalised CdS quantum dot

Chapter 5

5. CONCLUSIONS

Thus, CdS quantum dots have been synthesized using simple arrested precipitation method. The optical and photoluminescent properties of the synthesized quantum dots were studied at room temperature. The size of quantum dots was calculated by optical band gap and from powder XRD which are in good agreement with the same obtained from FESEM and atomic force microscopy (AFM). The stability of semiconductor nanocrystals was proved by zeta potential measurements.

The lactoferrin was successfully conjugated to the CdS quantum dots and was characterized with aforementioned techniques. The successful conjugation of lactoferrin on surface of CdS was proved by FT-IR studies as well as estimation of protein by Lowry's method. The absorption spectra of lactoferrin functionalised CdS quantum dot was considerable red shifted relative to bare CdS quantum dots indicating increased in size on conjugation.

An inhibition of growth of *E.coli* was observed for both CdS and lactoferrin conjugated CdS quantum dots albeit later showed more inhibition.

Chapter 6

6. REFERENCE

1. Reed M.A, Randall J.N., Aggarwal R.J, Matyi R.J, Moore T.M. and Wetsel A.E. Phys. Rev. Lett., 60, 535 (1988).

2. Kirstaedter, N., Lendentsov N.N., Grundmann M., Bimberg D., Ustinov V.M., Ruvimov S.S., Maximov M.V., Kopev P.S., Alferov Z.I., Richter U., Werner P., Gosele U. and Heydenreich. Electronics lett., 30, 1416 (1994).

3. Shoji H., Mukai K., Ohtsuka N, Sugawara M., Uchida T., and Ishikawa H., IEEE photonics technol. Lett, 7, 1385 (1985).

4. Hawrylak P., Palacios J.J., Phys. Rev. B51, 1769 (1995).

5. Rocksby H.P. J.Soc. Glass Tech.16, 171(1932).

6. Ekimov A.I, Efros Al. L and Onushchenko A.A., Sol. State Comm. 56, 921-924 (1985).

7. Reed M.A., Bate R. T., Bradshaw K., Duncan W.M., Frensley W.M., Lee J.W. and Smith H.D. J. Vaccum Technol. B, 4, 358 (1986).

8. Cibert J., Petroff P.M., Dolan G.J., Pearton C.J, Gossard A.C., English J.H. Appl. Phys. Lett. 49, 1275 (1986).

9. Temkin H., Dolan G., Panish M.B. and Chu S.N.G. Appl. Phys. Lett. 50, 413 (1987).

10. Kash K., Scherer A, Worlock J.M., Craighead H.G., and Tamargo M.C. Appl. Phys. Lett. 49, 1043, 473–476 (1986).

11. Ekimov A.I, Efros Al. L and Onushchenko A.A., Sol. State Comm. 56, 921-924 (1985).

12. Brus L.E., J. Chem. Phys. 79, 5566 (1983).

13. Reed M.A., Randall J.N., and A. E. Wetsel., *Phys. Rev. Lett.* **60**, 535 (1988).

14. Weller H., Koch U., Gutierrez M. And Henglein A., Ber. Bunsenges Phys.Chem., 88, 649 (1984).

15. http://public.itrs.net/

16. Brus L.E. J. Chem. Phys., 80, 4403 (1984).

17. Brus, L. E. J. Chem. Phys., 79, 5566 (1986).

18. Henglein A. and Bunsenges B., Phys. Chem., 86, 301 (1982).

19. Kuczynski C.C. and Thomas J.K., Chem. Phys. Lett., 88, 445 (1982).

20. Fox M.A. and Lindig B., Chem, J. Am. Chem. Soc., 104, 5828(1982).

21. Brus L.E., J. Chem. Phys., 79, 5566 (1983).

22. Ekimov A.I. and Onushchenko A.A., Sov. Phys.-Semiconductors. 16, 775 (1982).

23. Efros A.L., Sov. Phys. – Semiconductors. 16, 772 (1982).

24. Bruchez M.J., Moronne M., Gin P., Weiss S. and Alivisatos A.P., Science. 281, 2013 (1998).

25. Chan, W.C.W. and Nie, S., Science. 281, 2016 (1998)

26. Jaiswal J.K., Mattoussi H., Mauro J.M., Simon and S.M. Nature Biotechnology. 21, 47 (2003).

27. Santra S.,Yang H., Stanley J.T., Holloway P.H., Moudgil B.M., Walter G. and Mericle R.A. ChemCommun. 33, 3144 (2005).

28. Ballou B., Lagerholm B.C., Ernst L.A., Bruchez M.P., and Waggoner A.S. Bioconjugate Chemistry, 15, 79 (2004).

29. Gao X. and Nie S., Trends in Biotechnology, 21,9, 371 (2003).

30. Reed M.A, Randall J.N., Aggarwal R.J, Matyi R.J, Moore T.M. and Wetsel A.E. Phys. Rev. Lett., 60, 535 (1988).

31. Ashoori R.C., Stormer H.L., Weiner J.S., Pfeiffer L.N., Baldwin K.W. and West K.W. Phys. Rev. Lett., 68, 3088 (1992).

32. Ashoori R.C., Stormer H.L., Weiner J.S., Pfeiffer L.N., Baldwin K.W. and West K.W. Phys. Rev. Lett., 71, 613 (1993).

33. Hansen W., Smith T.P., Lee K.Y., Brum J.A., Knwdler C.M., Hang J.M. and Kern D.P. Phys. Rev. Lett., 62, 2168 (1989).

34. Lorke A., Kotthaus J.P., and Ploog K., Phys. Rev. Lett., 64, 2559 (1990).

35. Brunner K, Bockelmann U, Abstreiter G, Walther M, Böhm G, Tränkle G and Weimann G., Phys. Rev. Lett., 69, 3216 (1992).

36. Petroff P.M. and DenBaars S.P. Superlattices and Microstructures,15, 15 (1994).

37. Stranski I. N. and Krastanow L. Akad. Wiss. Wien Math.-Naturwiss. Kl. IIb 146 797 (1939).

38. Grundmann M., Stier O., and Bimberg D. Phys. Rev. B 52, 11, 969 (1995).

39. Kirstaedter, N., Ledentsov N., Grundmann M., Bimberg D., Ustinov V., Ruvimov S., Maximov M., Kopev P., and Alferov Z. Electronics Letters 30,1416 (1994).

40. Fafard S., Leon R., Leonard D., Merz J.L., and Petroff P.M. Phys. Rev. B 50, 8086 (1994)

41. Raymond S., Hawrylak P., Gould C., Zawadzki P., Sachrajda A., Charbonneau S., Fafard S., Leonard D., Petroff P.M. and Merz J.L. Solid State Commun., 101, 883 (1997).

42. Fukui T., Ando S., Tokura Y., and Toriyama T., Appl. Phys. Lett. 58, 2018 (1991).

43. Butty J., Hu Y. Z., Peyghambarian N., Kao Y. H. and Mackenzie J. D. Appl Phys Lett. 18, 67, 2672 (1995).

44.Yang H., Huang D., Wang X., Gu X., Wang F., Xie S.,Yao X. J Nanosci Nanotechnol. 5, 1737 (2005).

45. Sonochemistry and its Application in Materials Science. Aharon Gedanken.

46. Arora S. and Manoharan S.S. Journal of Physics and Chemistry of Solids., 68, 1897 (2007)

47. Murcia M.J., Shaw D.L., Woodruff H., Naumann C.A., Bruce A., Yong R. and Long E.C. Chem. Mater., 18, 2219 (2006).

48. Xiong H.M., Shchukin D.G., Möhwald H., Xu Y. and Xia Y.Y. Angew. Chem. Int. Ed., 48, 2727 (2009).

49. Li H.L., Zhu Y.C., Chen S.G., Palchik O., Xiong J.P., Koltypin Y., Gofer Y., and Gedanken A. J. Solid State Chem., 172, 102–110 (2003).

50. Zhang H., Sun P., Liu C., Gao H., Xu L., Fang J., Wang M., Liu J. and Xu S. ACS Nano., 3(6), 1580 (2009).

51. Li M., Ge Y., Chen Q., Xu S., Wang N. and Zhang X. Talanta., 72, 89 (2007).

52. Wei S., Lu J., Yu W. and Qian Y. J. Appl. Phys. 95, 3683 (2004).

53. Brus L.E. J. Chem. Phys., 80, 4403 (1984).

54. Wei S., Lu J. and Yu W. J. Appl Phy 7, 95 (2004).

55. Brus, L. E. J. Chem. Phys., 79, 5566 (1986).

56. Brus, L. E. IEEE J. Quantum Electronics. 22, 1909 (1986).

57. Hawrylak P. and Wojs A. Semicond. Sci. Technol., 11, 1516 (1996).

58. Lee S.J., Shin N.H., Kot J.J., Parkt M.J. and Kummel R. Semicond. Sci. Technol. 7, 1072 (1992).

59. Klein D.L., Roth R., Lim A.K., Alivisatos A. and McEuen P.L. Nature., 389, 699 (1997).

60. Henglein A., Gutierrez M., Weller H., Fojtik A. and Jirkovsky J. Ber. Bunsenges. Phys. Chem., 93, 593 (1989).

61. Murray C.B., Norris D.J. and Bawendi M.G. J. Am. Chem. Soc., 115, 8706 (1993).

62. Rossetti R., Nakahara S. and Brus L.E. J. Chem. Phys., 79, 1086 (1983).

63. Chandler R.R. and Coffer J.L. J. Phys. Chem., 97, 9767 (1993).

64. Rajh T., Micic O.I. and Nozik A.J. J. Phys. Chem., 97, 11999 (1993).

65. Rama Krishna M.V. and Friesner R.A. J. Chem. Phys., 95, 8309 (1991).

66. Lippens P.E. and Lannoo M. Phys. Rev. B, 39, 10935 (1989).

67. Lippens P.E. and Lannoo M. Phys. Rev. B, 41, 6079 (1990).

68. Brus L.E. J. Chem. Phys. 1984, 80, 4403.

69. Herron N., Calabrese J.C., Farneth W.E. and Wang Y. Science, 259, 1426 (1993).

70. Rogach A.L., Kornowski A., Gao M., Eychmuller A. and Weller H. J. Phys. Chem. B, 103, 3065 (1999).

71. Rogach A.L., Katsikas L., Kornowski A., Su D.S., Eychmuller A. and Weller H. Ber. Bunsenges. Phys. Chem., 100, 1772 (1996).

72. Rogach A.L., Katsikas L., Kornowski A., Su D., Eychmuller A. and Weller H. Ber. Bunsenges. Phys.Chem., 101, 1668 (1997).

73. Gao M., Kirstein S, Mohwald H., Rogach A.L., Kornowski A., Eychmuller A. and Weller H., J. Phys.Chem., 102, 8360 (1998).

74. Rogach A.L., Kershaw S.V., Burt M., Harrison M., Kornowski A., Eychmuller A. and Weller H. Adv.Mater., 11, 552 (1999).

75. Kershaw S.V., Burt M., Harrison M., Rogach A.L., Weller H. and Eychmuller A., Appl. Phys. Lett., 75, 1694 (1999).

76. Hoppe K., Geidel E., Weller H.and Eychmuller A., Phys. Chem. Chem. Phys., 4, 1704 (2002).

77. Mostafavi M., Liu Y., Pernot P. and Belloni J., Rad. Phys. Chem., 59, 49 (2002).

78. Gaponik N.P., Talapin D.V., Rogach A.L., Hoppe K., Shevchenko E.V., Kornowski A., Eychmuller A. and Weller H., J. Phys.Chem. B, 106, 7177 (2000).

79. Rockenberger J., Troger L., Kornowski A., Vossmeyer T., Eychmuller A., Feldhaus J. and Weller H., J. Phys. Chem. B, 101, 2691 (1997).

80. Rockenberger J., Troger L., Rogach A.L., Tischer M., Grundmann M., Weller H., Eychmuller A., Ber. Bunsenges. Phys. Chem., 102, 1561 (1998).